UNIVERSITÀ DEGLI STUDI DI PADOVA

DEPARTMENT OF INFORMATION ENGINEERING

Master Thesis in

TELECOMMUNICATION ENGINEERING

A Simulation Study of Cell-Search Techniques in 5G Millimeter-Wave Cellular Networks

Supervisor
Prof. Michele Zorzi

Master candidate
Marco Giordani

12th October, 2015

Academic Year 2014/2015

Dedico questa tesi ai miei genitori,
che da sempre mi sostengono con affetto...

Abstract

The fifth generation of mobile technology (5G) is positioned to address the demands and business contexts of 2020 and beyond. It is expected to enable a fully mobile and connected society, related to the tremendous growth in connectivity and density/volume of traffic that will be required in the near future.
Among all the challenges that will be faced, a very relevant one is referred to the definition of new control procedures, related to the Physical Control Plane, such as Cell-Search, which go beyond what existing mobile technologies (such as current 4G-LTE cellular networks and its enhancements) can support.
In this thesis, we aim at studying these problems, comparing all the existing solutions, highlighting pros and cons and finding new valid approaches, in order to make a contribution to the research that, in the next years, will be very actively conducted all over the world. One of the goal is to simulate those algorithms through the open-source and discrete-event network simulator NS-3, implementing different scenarios where Cell-Search procedures will be tested and analysed.
The simulated scenarios will be deeply examined through figures and graphs which will be used to compare all the procedures' performances.

Sommario

La tecnologia cellulare di quinta generazione (5G) nasce per far fronte alle esigenze, non soltanto aziendali, legate all'enorme crescita di connettività e densità di traffico che sarà una realtà nel prossimo futuro.
Tra tutte le sfide che si dovranno affrontare, trova particolare rilevanza la definizione di nuove procedure di controllo, a livello fisico, come la procedura di Cell-Search, che vanno al di là di ciò che le esistenti tecnologie mobili (come l'attuale rete cellulare 4G-LTE e i suoi relativi potenziamenti) possono supportare.
In questa tesi, tali problematiche saranno profondamente studiate, facendo un confronto tra le soluzioni esistenti, sottolineandone vantaggi e svantaggi, e determinando nuovi validi approcci, al fine di contribuire alla ricerca che, nei prossimi anni, sarà attivamente condotta in tutto il mondo. Uno degli obiettivi principali sarà quello di simulare i vari algoritmi facendo uso del simulatore a eventi discreti NS-3, implementando diversi scenari in cui le procedure di Cell-Search saranno testate e analizzate.
Gli scenari simualati saranno attentamente esaminati attraverso lo studio di figure e grafici, che permetteranno di mettere in relazione le prestazioni delle varie tecniche.

Contents

List of Figures

List of Tables

List of Acronyms

P_{MD}	Miss-detection probability
μW	Micro-wave
AMC	Adaptive Modulation and Coding
AoA	Angles of Arrival
AoG	Angles of Arrival
BF	Beamforming
BS	Base Station
CDF	Cumulative Distribution Function
CQI	Channel Quality Indicator
CS	Cell-Search
D2D	Device-to-Device
DL	Downlink
DT	Discovery Time
FDD	Frequency Division Duplex
HetNet	Heterogeneous Network
IA	Initial-Access
LoS	Line of Sight
LTE	Long Term Evolution
MIMO	Multiple-Input-Multiple-Output

mmW	Millimeter-wave
NLoS	Non Line of Sight
NYU	New York University
OFDM	Orthogonal Frequency Division Multiplexing
PHY	Physical (Layer)
PSS	Primary Synchronization Signal
QoE	Quality of Experience
RAT	Radio Access Technologies
RA	Random-Access
RF	Radio Frequency
RSRP	Reference Signal Received Power
SAP	Service Access Point
SINR	Signal to Interference and Noise Ratio
SSS	Secondary Synchronization Signal
TB	Transport Block
TDD	Time Division Duplex
UE	User Equipment
ULA	Uniform Linear Array
UL	Uplink

Chapter 1

Introduction

From analogue through to Long Term Evolution (LTE) , each generation of mobile technology has been motivated by the need to meet a requirement identified between that technology and its predecessor. The fifth generation of mobile technology (5G) is positioned to address the demands and business contexts of 2020 and beyond. It is expected to enable a fully mobile and connected society, related to the tremendous growth in connectivity and density/volume of traffic that will be required in the near future [8]. In according to the Cisco Visual Networking Index (VNI) [1], it is expected, as in Figure 1.1, that global mobile data traffic will grow at a Compound Annual Growth Rate (CAGR) of 57 percent from 2014 to 2019, reaching 24.3 exabytes per month by 2019, and mobile devices and connections will grow to 11.5 billion within the next four years, exceeding the world's projected population at that time (7.6 billion).

In order to face this continuing growth in demand from subscribers for better mobile broadband experiences, there is a need to push the performance to provide, for example:

- much greater throughput, at least 1 Gb/s or more data rates, to support ultra-high definition video and virtual reality applications;
- much lower latency, less than 1 ms, to support real time mobile control and Device-to-Device (D2D) applications and communications;

[1] The Cisco Visual Networking Index (VNI) Global Mobile Data Traffic Forecast Update is part of the comprehensive Cisco VNI Forecast [1], an ongoing initiative to track and forecast the impact of visual networking applications on global networks, presenting some of Cisco's major global mobile data traffic projections and growth trends.

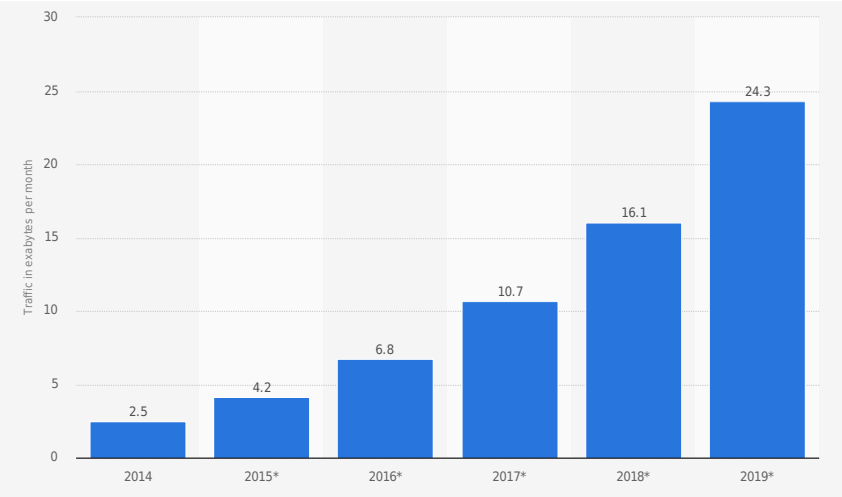

Fig. 1.1: Global mobile data traffic from 2014 to 2019 (in exabytes per month). Figure from [1].

- ultra-high reliability;
- much higher connectivity density;
- higher mobility range;
- lower energy consumption, reduced by a factor of 1000, to improve upon connected device battery life.

All these items are deeply analysed, for example, in the Nokia [2] and Huawei [9] White Papers, as summarised in Figure 1.2.

In fact, many enterprises, companies and research institutes are investing effort, time and money in defining new standards to create a high performance 5G environment, to meet market demands within 2020, which goes beyond what existing mobile technologies (such as current 4G-LTE cellular networks and its enhancements) can support.

In order to deal with those requirements, some key aspects have been identified that will make this future network a reality [2].

Since current micro-wave (μW) spectrum under 5 GHz is very fragmented and crowded and given the abundance of spectrum available in the cm-wave and mm-wave bands, there are significant research efforts into using these bands, especially the millimeter-wave (mmW) one [10] between 30 GHz and 300 GHz, to be employed for future cellular networks. This

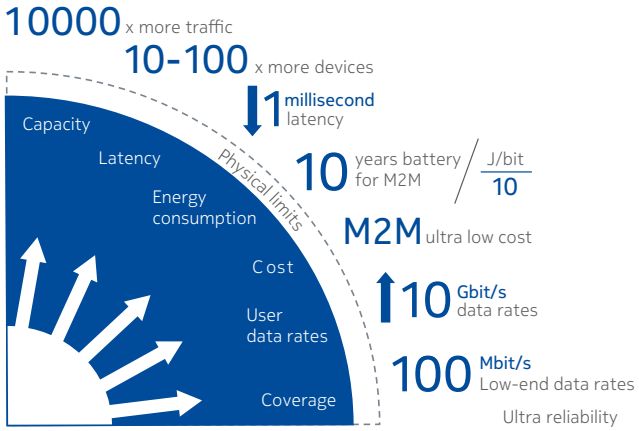

Fig. 1.2: 5G future requirements. Figure from [2].

will permit also to increase the data rate to levels that are even unimaginable for current systems. On the one hand, with the increasing carrier frequency, the propagation conditions become more demanding than at the lower frequencies traditionally used for wireless services, but advances in technology development such as massive Multiple-Input-Multiple-Output (MIMO) techniques and beamforming (BF) will realize their full potential when taking advantage of the short wavelengths, permitting to support the required very high data rates [11].

The second pillar of 5G will be to use many more base stations (BS), deployed in a heterogeneous network (HetNet), combining macro sites with smaller base stations and using a wide range of radio technologies. These will include LTE, Wi-Fi and any future 5G technologies, integrated flexibly in any combination.

Another aspect will be to get the best possible network performance by evolving existing Radio Access Technologies (RAT), towards new 5G wireless ones.

Among all the challenges that will be faced, a very relevant one is referred to the definition of new control procedures, related to the Physical Control Plane, such as synchronization, Cell-Search (CS) , initial and random access, user association. Theses procedures, currently implemented in traditional cellular systems, must be reviewed, due to important issues and differences that have to be analysed and deeply examined. To address those problems, different approaches will be taken into account, and re-

search challenges will be discussed. These issues have not been thoroughly investigated in the literature yet, but will become a real urgent scientific topic, in the foreseeable future.

This thesis aims at studying these problems, comparing all the existing solutions, highlighting pros and cons and finding new valid approaches, in order to make a contribution to the research that, in the next years, will be very actively conducted all over the world.

One of the goals is to simulate those algorithms through the open-source and discrete-event network simulator NS-3 [12], implementing different scenarios where Cell-Search procedures will be tested and analysed.

More specifically, the thesis is organized as follows.

- Chapter 2 explains in detail the main features of the upcoming 5G cellular networks, analyse the main drawbacks and issues we will face, when working at the new mmW frequency band;
- in Chapter 3, after a brief description of the Initial-Access (IA) procedure, implemented in the current 4G-LTE systems, we will list the aspects that cannot be entirely reused in the mmW networks and we will understand how to deal with those limitations;
- in Chapter 4, we will describe the NS-3 modules we will use to simulate the CS algorithms, giving an overview of how the framework is structured and how it works;
- Chapter 5 aims at exposing what are the Cell-Search procedures that have been proposed as a standard for future 5G networks. We will then describe two techniques that we will compare under many metrics, referring also to the NS-3 modifications we have made to the code, in order to implement said algorithms;
- Chapter 6 presents the simulation scenarios we have implemented, providing figures and results which will be used to compare the different techniques;
- finally, in Chapter 7, future works are presented, listing further analysis that could be made and concluding the thesis.

Chapter 2

5G cellular systems

2.1 5G: basic overview

As described in Chapter 1, the increasing internet data traffic has driven the capacity demands for currently deployed 3G and 4G wireless technologies; intensive research toward 5th generation wireless communication networks is thus progressing on many fronts, since 5G technology is expected to be in use even before 2020 (for examples, the South Korean market leader, *SK Telecom*, signed a very ambitious agreement with Ericsson to develop 5G technology in time to demonstrate a network at the 2018 Winter Olympics in Pyeongchang [8]).

2.1.1 5G Key Enabling Technologies

Groundbreaking innovations will drive 5G technologies to meet the unprecedented speeds, near-wireline latencies, ubiquitous connectivity with uniform Quality of Experience (QoE) , and the ability to connect massive amounts of devices with each other, all working in unison to provide the user with an immersive experience, even while the user is on the move. Future 5G systems will encompass fundamentally new designs to boost wireless capacity utilizing new frequency bands, advanced spectrum efficiency enhancement methods in the legacy band, and seamless integration of licensed and unlicensed bands [3].

Figure 2.1 shows an overview of the key enabling technologies that will permit to reach the 5G main requirements of Figure 1.2.

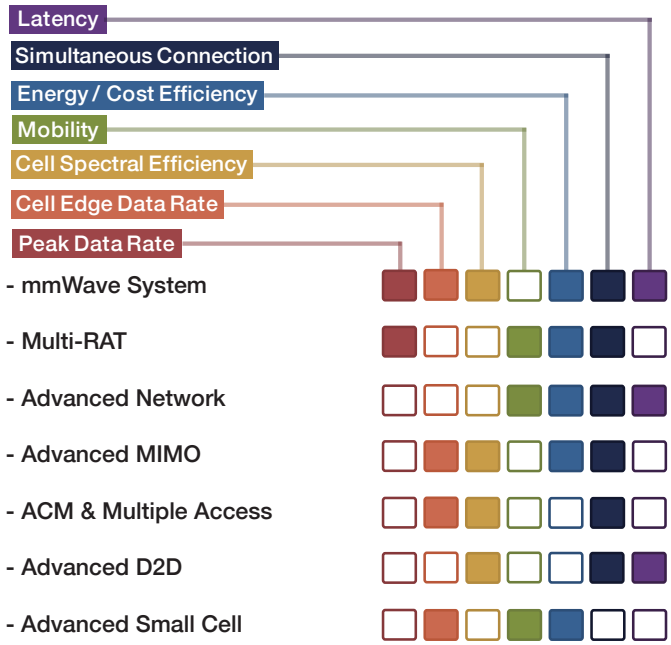

Fig. 2.1: Overview of 5G Key Enabling Technologies. Figure from [3].

Therefore, the massively higher capacity needs of the 5G systems will be addressed by the following technologies.

Millimeter-wave systems This concept will be further studied in Section 2.2.

HetNet In order to provide a ubiquitous high QoE gigabit accessibility, 5G small cells can be coupled with the overlaid 4G macro cells. These *picocells* or *femtocelles* are covered by low-power and low-cost BSs relaying on the same backhaul and access features as macrocells. They primarily provide multi-gigabit per second throughput with high QoE to mobile users over the bands above 6 GHz [13].

Meanwhile, the 4G BS can serve as a control channel to 5G cells, exploiting the legacy spectrum, to maintain the connection, to perform handover, to provide real-time services.

Massive MIMO MIMO systems experience small inter-user and inter-cell interferences and consequently achieve significantly higher throughput than the state-of-the-art systems. One of the main challenges to build

massive MIMO systems in practice is the limitation in the number of antennas that can be equipped at a BS: at the mmW frequencies, a large number of antenna elements can be packed into a small form factor due to the much smaller wavelength than legacy cellular bands. Therefore, MIMO systems allow to produce large beamforming gain, implementing a highly directional transmission through narrow beams, which permits both to make the path loss of mmW transmission comparable to those of typical cellular frequency bands and to alleviate the co-channel interference issue, significantly increasing the spatial reuse gain [14]. Consequently, BSs having large antenna arrays are capable of serving more users, thus Massive MIMO exhibits a high spectrum efficiency, which substantially improves the throughput [15].

Multi-Radio Access Technology (Multi-RAT) By interworking and integrating the 5G system with other RATs, the upcoming systems will be able to take advantage of the unique characteristics of each RAT and improve the practicality of the system as a whole. For example, integration including carrier aggregation of licensed and unlicensed bands will help in increasing the available system bandwidth [3].

Advanced Device-to-Device This technology allows a User Equipment (UE) to communicate with another UE in proximity directly over a D2D link, without extra hops through the central BS, offloading data from network [14]. It can help to reduce the communications latency and support larger number of simultaneous connections in a network.

Physical Layer Spectral efficiency could be further improved upon if the requirements of strict orthogonality were relaxed. Several modified multicarrier transmission schemes are under consideration for 5G radio access [16].

Advanced Networks Novel topologies, such as Software-Defined Networking (SDN) [17], where network control is decoupled from forwarding and is directly programmable, or Network Functions Virtualization (NFV) [18], which aims at implementing the network functions in software,

without the need of installation of new equipment, will contribute to significantly reduce the network latency, lowering also costs and complexity.

Energy Harvesting Networks Energy harvesting is highly desirable both for prolonging the battery life and for improving the energy efficiency of networks. BSs and UEs may harvest renewable energy from the environment, such as solar energy or wind energy, or from ambient radio signals (simultaneous wireless information and power transfer is envisaged as a promising technology for 5G wireless networks) [19].

All the items described above are only a part of the fundamental aspects that need to be further explored in the near future, in order to meet all the requirements we have considered in the analysis. In the next section, we will particularly investigate what are pros and cons of one of the most important 5G key enabling technology, i.e., the millimeter-waves.

2.2 Millimeter-waves in 5G

According to what has been introduced in Chapter 1, the millimeter-wave band refers to the frequency range from 30 GHz to 300 GHz (or often from 10 GHz to 300 GHz), which is the highest electromagnetic radiation radio frequency band, with wavelengths ranging from 1 to 100 mm [20].

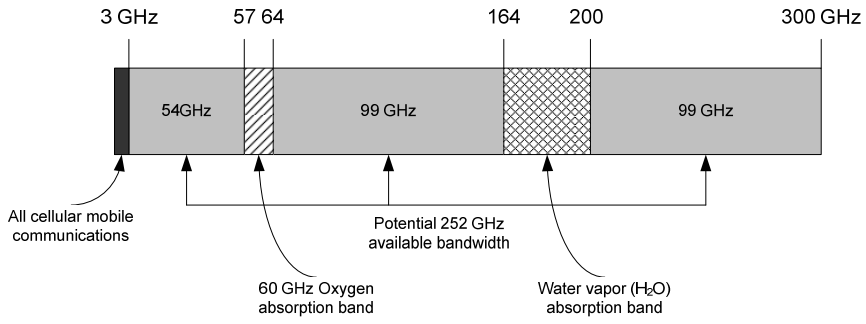

Fig. 2.2: Millimeter-wave spectrum. Figure from [4].

There are several motivations and advantages to utilize mmW frequencies in future 5G networks. As already described before, the enormous amount of available spectrum, differently from the current cellular systems

below 3 GHz, can support the higher data rates required in future mobile broadband access networks. The physical size of antennas at mmW frequencies is so small that it becomes practical to build complex antenna arrays (such as MIMO systems), in order to obtain high antenna gains increasing the overall performances. Again, inherent security and privacy of mmW transmissions are improved because of the limited transmission range and the relatively narrow beam widths that can be achieved [14].

Although this new band has gained great interest for 5G cellular systems, there are many concerns about its transmission characteristics, as explained in the next subsection.

2.2.1 Propagation characteristics

Free-space Losses

Transmission loss of millimeter wave is accounted for principally by *free space loss*. Traditionally, the *Friis* transmission law gives us the following equation:

$$\frac{P_r}{P_t} = G_t G_r \left(\frac{\lambda}{4\pi R} \right)^2 \tag{2.1}$$

where P_r and P_t are the received and transmit powers, respectively, G_t and G_r are the antenna gains of the transmit and receive antennas, respectively, λ is the wavelength and R is the distance between the transmitter and receiver. A direct result of (2.1) is that the free-space path gain scales as λ^2. Hence, for mmW bands, due to high frequency and, consequently, to the small wavelength, the communications will suffer from high path loss.

Moreover, it should be noticed that, for a directive antenna, the gain G is given by:

$$G = \frac{4\pi}{\lambda^2} A_{\text{eff}} \tag{2.2}$$

where A_{eff} is the antenna aperture of the effective area. If both the transmit and receive antenna apertures are held constant, the link budget actually increases with the frequency, mitigating the higher noise floor associated with broader signal bandwidths. Therefore, the use of higher frequencies should not have any inherent disadvantage compared to lower frequencies, in terms of free space loss [20]. Again, also MIMO BF gain contributes

to reduce this high path loss effect, recovering an acceptable transmission range.

Atmospheric Gaseous Losses

Atmospheric gaseous losses of millimeter-wave transmissions due to oxygen molecule (O_2) and water vapor (H_2O) absorption, actually only at some frequencies (respectively around 60 GHz and 180 GHz, as in Figure 2.3), results in high attenuation of the radio signal.

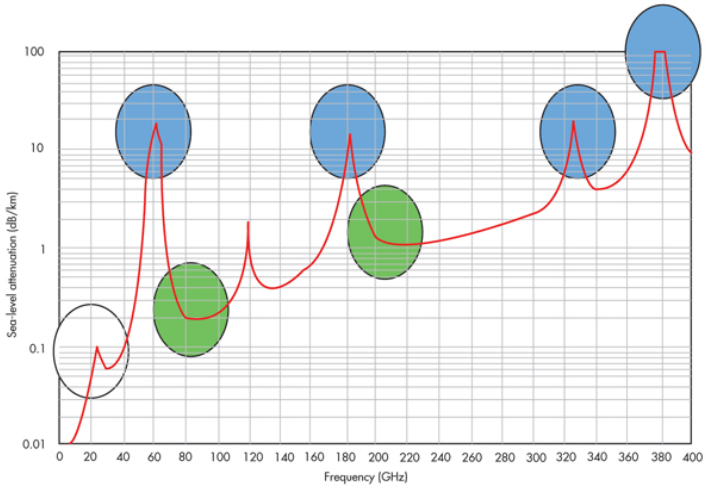

Fig. 2.3: Millimeter-wave propagation characteristics, due to atmospheric gases.

Nevertheless, beyond those absorption bands (that should be thus avoided when transmitting), the other spectral regions of mmW are not heavily affected by gaseous losses [14].

Rain Losses

MmW propagation is also affected by rain. Raindrops are roughly the same size as the radio wavelengths and, therefore, cause scattering of the radio signal [21]. The attenuation (dB per km) can be calculated from rain rates (mm per hour), and the curves are plotted in Figure 2.4. Fortunately, the most intense rain tends to fall in selected countries of the world and happens in short bursts, while light rain yields just a little attenuation [4]. Considering that today's cell sizes in urban environments are on the order of 200 meters [14], rain attenuation will present a minimal impact on mmW propagation.

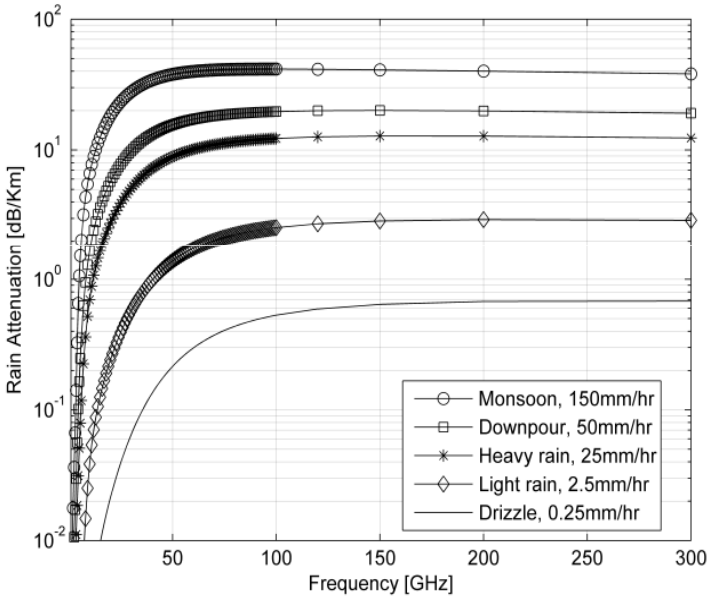

Fig. 2.4: Rain attenuations at 1-300 GHz frequencies. Figure from [4].

Penetration Losses

While signals at lower frequencies can penetrate more easily through buildings, mmW signals do not penetrate most solid materials very well, due to their small wavelengths. For example, as reported in [4], these signals would not be able to penetrate through solid buildings made of brick or concrete (but they might eventually reach inside the buildings through glass windows and doors).

High attenuations for certain materials may aid in keeping mmW signals transmitted from outdoor base stations confined to streets and other outdoor structures. The indoor coverage in this case can be provided by other means such as using indoor Wi-Fi or femtocell solutions.

Also foliage losses at millimeter wave frequencies are significant. In fact, foliage loss may be limiting propagation impairment in some cases [21]. As we can see in Figure 2.5, at 80 GHz frequency and 10 meters foliage penetration, the loss can be about 23.5 dB, which is about 15 dB higher compared to the loss at 3 GHz frequency [4].

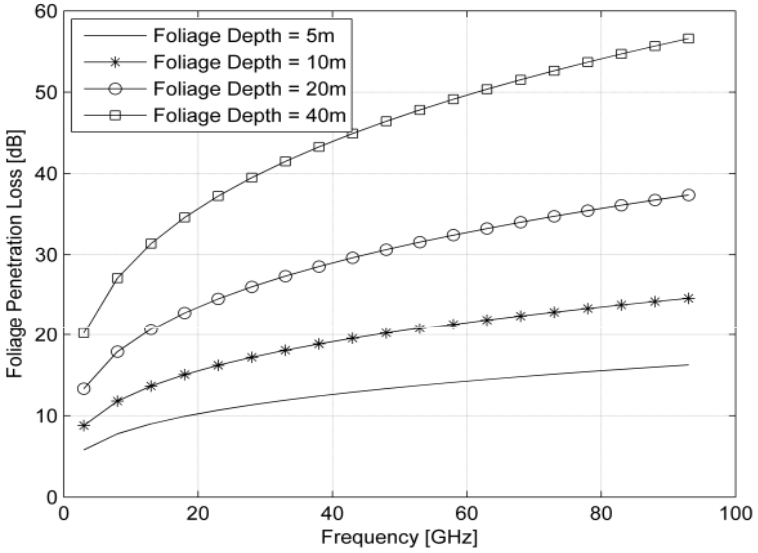

Fig. 2.5: Foliage penetration loss at 1-100 GHz frequencies. Figure from [4].

In rural areas, where forest exists, we can therefore expect that millimeter-wave signals would be severely attenuated, provoking undesired blockage effects.

Scattering/Diffraction

If there is no Line of Sight (LoS) path between the transmitter and the receiver, the signal may still reach the receiver via reflections from objects in the proximity of the receiver or via diffraction. The short wavelengths of millimeter-wave signals result in low diffraction, but are more subjected to *shadowing* and reflection [21].

Moeover, shorter wavelengths, related to higher frequencies, cause the reflecting material to appear relatively *rougher*, which results also in greater *diffusion* of the signal and less specular reflection. Therefore, [22] shows that the Non Line of Sight (NLoS) propagation suffers from high attenuation: new path loss models for NLoS situations are then needed for millimeter bands.

Chapter 3

Initial Access: 4G-LTE vs 5G

In all mobile communication systems, when a terminal switches on (or when it has lost the connection to a serving cell), it must perform certain steps before it can receive or transmit data. These phases, which constitute the Initial-Access (IA) procedure, can be categorized into 3 main stages: Cell-Search, extraction of system information and Random Access (RA) .

In this chapter, we will review Initial Access in traditional 4G-LTE cellular networks, in order to better understand its related issues in millimeter-wave systems.

3.1 Initial-Access procedure in 4G-LTE

This section describes the necessary procedures for a terminal to access an LTE-based network, according to the description in Chapters 7 and 19 of [5] and in Chapter 18 of [23].

3.1.1 Cell-Search in LTE

Cell-Search aims at detecting surrounding cells and measuring the strength of received signal from each of these cells. One of them will become the UE's entry point to join the network. This is done by synchronizing to each available frequency in the network and checking whether this is a frequency from the right operator which it wants to connect to.

This synchronization procedure makes use of two specially designed

physical signals which are broadcast omnidirectionally in the downlink by the BS in each cell: the Primary Synchronization Signal (PSS) and the Secondary Synchronization Signal (SSS) . Each UE in the cell is aware a priori of when and where the synchronization control channel is and, thereby, it can extract and detect those signals.

Once the terminal has detected and identified the PSS of the cell, it has found its timing and thus also the position of the SSS which has a fixed offset, relative to the PSS, within the frame.

Then, the detection of the SSS not only enables time and frequency synchronization, but also provides the UE with the physical layer identity of the cell and the cyclic prefix length, and informs it whether the cell uses Frequency Division Duplex (FDD) or Time Division Duplex (TDD) .

Since, usually, multiple neighbour BSs send their own PSS and SSS messages, by using the measured Reference Signal Received Power (RSRP)[1] , the PHY entity of each UE is able to generate a list of detected cells, each with its corresponding cell ID and averaged RSRP. Finally, inspecting the report, the terminal can choose the cell with the strongest RSRP (*max-RSRP rule*), instructing back its PHY entity to synchronize to this particular cell.

After this phase, the UE can start the channel estimation.

3.1.2 System information in LTE

At this moment, the terminal has to acquire the cell system information. This information is repeatedly broadcast by the network and needs to be acquired by terminals in order for them to access and, in general, operate properly within the network and a specific cell. The system information includes, among other things, downlink and uplink cell bandwidths, the uplink/downlink configuration in case of TDD, detailed parameters related to Random-Access transmission, number of transmit antennas and uplink power control, etc.

In LTE, system information is delivered by two different mechanisms relying on two different transport channels:

[1]RSRP is the linear average of the downlink reference signals across the channel bandwidth and provides information about signal strength, without giving any indication of signal quality.

- A limited amount of system information, corresponding to the so-called Master Information Block (MIB), is transmitted using the Physical Broadcast CHannel (PBCH);
- the main part of the system information, corresponding to different so-called System Information Blocks (SIBs), is transmitted using the Downlink Shared CHannel (DL-SCH).

Once the right synchronization information has been extracted, the next step is to inform the network, for the first time, that the UE is trying to get access.

3.1.3 Random Access in LTE

At this stage, the UE does not have any resource or channel available to inform the network about its desire to connect to it; the LTE Random Access CHannel (RACH) therefore plays a key role to perform this connection.

The LTE, RA procedure comes in two forms, allowing access to be either contention-based (implying an inherent risk of collision) or contention-free.

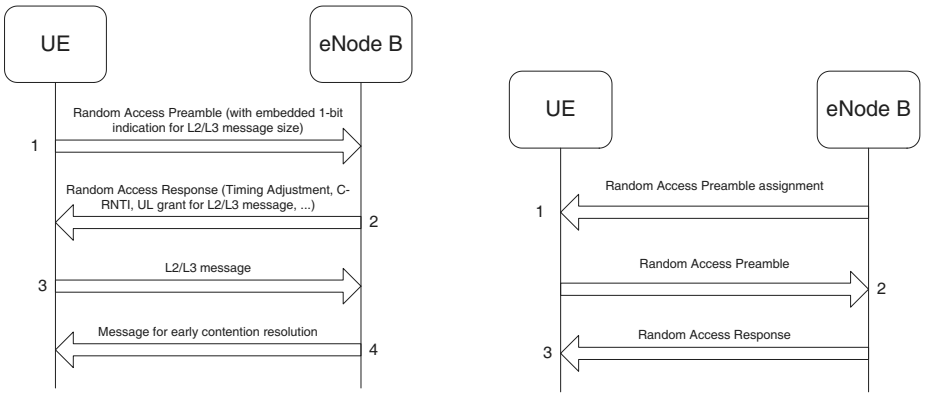

(a) *Contention-based procedure.* **(b)** *Contention-free procedure.*

Fig. 3.1: Random-Access procedures in 4G-LTE. Figure from [5].

Contention-based procedure

In the contention-based procedure, a RA preamble signature is randomly chosen by the UE, with the result that it is possible for more than one UE to transmit simultaneously the same signature, leading to the need for a

subsequent *contention resolution* process. The procedure consists of four steps, as shown in Figure 3.1(a).

Step 1 - Preamble transmission The UE selects randomly one contention-based signature (PRACH) and sends it to the BS.

Step 2 - Random-Access response The BS sends back to the UE, on the Physical Downlink Shared CHannel (PDSCH), a Random-Access response (RAR), which contains the Random-Access Radio Network Temporary Identifier (RA-RNTI), identifying the time-frequency slot in which the preamble was detected. The RAR conveys also a timing alignment instruction to synchronize subsequent uplink transmissions from the UE, an initial uplink resource grant for transmission of the Step 3 message, and an assignment of a Cell Radio Network Temporary Identifier (C-RNTI).

The UE expects to receive the RAR within a RA window time (the value of the window was communicated by the BS during the synchronization phase). If the UE does not receive a RAR within the configured RA time, it retransmits the preamble, with increased power.

Step 3 - Layer 2/Layer 3 (L2/L3) Message If RAR is correctly received the UE, on the Physical Uplink Shared CHannel (PUSCH), conveys the actual Random-Access procedure message (RRC), together with its identity C-RNTI, assigned in the RAR message.

In case of a preamble collision having occurred at Step 1, the colliding UEs will receive the same Temporary C-RNTI through the RAR and will also collide in the same uplink time-frequency resources when transmitting their RRC. This may result in such interference that no colliding UEs can be decoded by the BS, so that they restart the RA procedure. However, if one UE is successfully decoded by the BS, the contention remains unresolved only for the other UEs.

Step 4 - Contention Resolution Message The BS sends a message addressed to a certain C-RNTI. If the UE is able to receive this message and detects its own identity, it sends back a positive ACK, concluding the RA procedure. Otherwise, if the UE receives the message but detects another UE's

identity or fails to decode it, then it does not send anything back (DXT), exits the RA procedure and starts another one.

Contention-free procedure

In this kind of procedure, a dedicated signature is allocated to a certain UE. In such a way, the whole procedure is faster than the contention-based one. The steps are the same as before, but now, as shown in Figure 3.1, the procedure terminates with the RAR.

3.2 Initial Access in 5G: main limitations

The IA procedure that has been described in the previous section cannot be entirely reused in the upcoming mmW cellular systems, due to many aspects, as described below.

Range mismatch In LTE systems, acquiring time-frequency domain synchronization during Cell-Search is facilitated, since synchronization signals are transmitted omnidirectionally in the downlink, and current cellular networks use beamforming only after the physical-layer access has been established. On the other hand, in the mmW range, it may be essential to exploit beamforming even during the CS procedure. Otherwise, using omnidirectional transmission in the first stages, the availability of high antenna gains (BF) only in the data transmission plane would create a *mismatch* between the range at which a cell can be detected and the range at which reasonable data rates can be achieved, as in Figure 3.2.

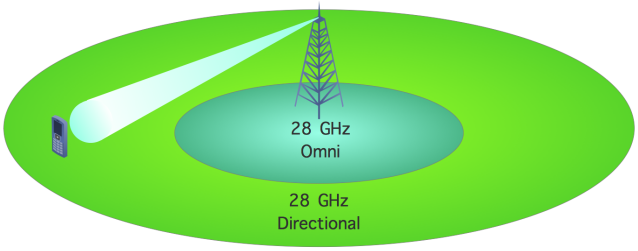

Fig. 3.2: Illustration of mismatch between discoverable area and actual supportable area at mmW band.

This disparity would in turn create a large area where a mobile user

may potentially be able to obtain a high data rate, but cannot realize this rate, since it cannot even be detected by the BS [24]. In [25], it has been shown that the data range can be at least 4 times larger than the synchronization range, even in a severely attenuated propagation environment.

This is caused by the fact that, as we pointed out in Section 2.2, bad performance of mmW communication, due to high path loss, can be attenuated by exploiting the BF gain. However, if transmitting the synchronizing signals omnidirectionally, we lose this advantage and the communication range results to be very poor, if compared to a directional mmW transmission.

Dedicated control channels LTE embeds system information (exchanged in the first stages of the Initial-Access procedure) in the MIB. While dedicated control channels can be established with omnidirectional communications, a UE still needs to decode a directional shared channel to extract system information in a mmW cellular network [25].

Spectrum efficiency We have seen before that, for systems operating at mmW bands, if the old LTE cell discovery technique is used, the discoverable area would be much smaller than the actual supportable area, due to the high pathloss at the mmWave frequency band. To ensure sufficient coverage, the mmW small cell should be deployed in a much denser way than what is actually needed. This will result in an inefficient use of the spectrum resource, low energy efficiency and high deployment capital cost; the reuse of the LTE methods cannot be efficiently implemented, but more sophisticated enhancements are needed.

Deafness and blockage It has been pointed that, in the contention-based Random-Access procedure of LTE, a UE triggers a timer after sending a preamble and, if no response is received from the BS in Step 3, it retransmits the preamble with an increased transmission power and/or after a random waiting (backoff) time. On the other hand, in a millimeter-wave cellular network, a RAR may not be received even if no collisions happen, due to *deafness* and *blockage* phenomena. Deafness refers to the situation in which the main beams of the transmitter and the receiver do not point to each other, while blockage refers to situation in which a message cannot

be delivered due to high attenuation of obstacles in the path. These situations cannot be solved by increasing the transmission power or waiting for a random backoff time (as in LTE), and so there must be used new ad-hoc techniques to distinguish real collision events from deafness and blockage.

HetNets limitations The conventional max-RSRP user association rule is unsuitable for 5G HetNets, since the transmit power disparity of macrocells (at μW) and small cells (at mmW) will lead to the association of most of the users with the macro BS, hence potentially resulting in inefficient small cell deployment. Moreover, the inherent nature of HetNets manifests itself in terms of the uplink-downlink asymmetry (the optimal user association for downlink or uplink can be less effective for the opposite direction [26]), backhaul bottleneck (densely deployed small BSs may introduce overwhelming traffic augments for the backhaul link and current small cell backhaul solutions cannot provide sufficiently large data rate [27]), mobility support (user association without considering user mobility may result in frequent handovers among the cells in HetNets [28]).

3.3 Initial Access in 5G

All the considerations of the previous section make us understand the need to review all existing models (as the ones of LTE), adapting them to the upcoming mmW cellular systems, in order to overcome the problems described. New algorithms and new methods must be studied, keeping in mind that a fully-directional data plane (as the one we want to implement for mmW cellular systems) demands also a directional (or at least hybrid) Cell-Search procedure in the new frequency band. Since compensating the high pathloss is not realistically achievable with precoding procedures, a practical solution is to use beamforming even in the first stages of the Initial-Access procedure.

On the other hand, directionality means that only one direction per time can be considered, with consequently delay issues that must be taken into consideration.

Moreover, if obstacles are not a limitation for current LTE communications (since microwaves can easily penetrate through solid materials while high frequencies are absorbed), when working at mmW this may be a non

negligible impairment.

In the next chapters, all those challenges will be considered and we will propose and study different solutions that try to overcome the identified issues for Cell-Search procedure in upcoming 5G millimeter-wave cellular networks.

Chapter 4

The NS-3 Network Simulator

4.1 Introduction to NS-3

The NS-3 simulator is a discrete-event network simulator targeted primarily for research and educational use. The NS-3 project is committed to build a solid simulation core that is well documented, easy to use and debug, and that caters to the needs of the entire simulation workflow, from simulation configuration to trace collection and analysis [12]. It currently implements a wide range of network protocols across various layers of the communication network. In order to simulate scenarios where UEs and BSs are deployed in macro-cells operating at the current cellular system's frequencies around 2 GHz, the simulator makes available the LENA modules [29]. They have been designed with a product-oriented perspective in order to allow users to test network algorithms in a simulation environment before they are deployed in the field.

However, since many LTE models cannot be entirely reused in the mmW scenarios, there was the need to test and implement also new NS-3 modules which could be perfectly designed and adaptable for the new frequency band with which users will work, and which take into account all the differences and divergences with the existing simulation solutions.

Lately, in May 2015, the New York University (NYU) Wireless research group [30] has developed a first version of such modules [31], creating a customizable model where the user can plug in various parameters, like carrier frequency, bandwidth, frame structure, etc., describing the behaviour of the millimeter wave channel and devices.

In this Chapter, we will describe in detail how those modules work, while in Chapter 5 we will extend them, in order to simulate with this software the CS procedures we are going to theoretically explain.

4.2 NS-3 modules description

The mmW modules provided by the NYU research group include: propagation model, channel model, physical (PHY) layer and MAC layer. All the framework, developed in C++, is inspired by the NS-3 LENA modules and provides compatibility with the entire NS-3 world. In the following subsections, we discuss the architecture of said modules, according to paper [31].

4.2.1 Physical (PHY) Layer - Introduction

The PHY layer implemented in the modules is completed with some features that can be manually set for creating scenarios to simulate. Among all the features that the PHY layer provides, we focus on: a fully customizable TDD frame structure[1], a radio characterization along with supporting MIMO techniques such as BF, a decoding error model at the receiver side and an interference model.

Frame Structure

The TDD frame structure is organized as follows. Each frame is subdivided into a number of subframes of fixed length specified by the user. Each subframe in turn is split into a number of slots of fixed duration. Each slot comprises a specific number of Orthogonal Frequency Division Multiplexing (OFDM) symbols. A slot can be used for either control (c) or data (d), and assigned for either uplink (UL) or downlink (DL) .

By default, the frame structure is set according to Figure 4.1 [2].
In the time domain, the frame is subdivided as in Table 4.1:

[1] In [32], it is assumed a dynamic time division duplex system as standard in mmW networks.

[2] The frame parameters are fully customizable in the *mmWavePhyMacCommon* class.

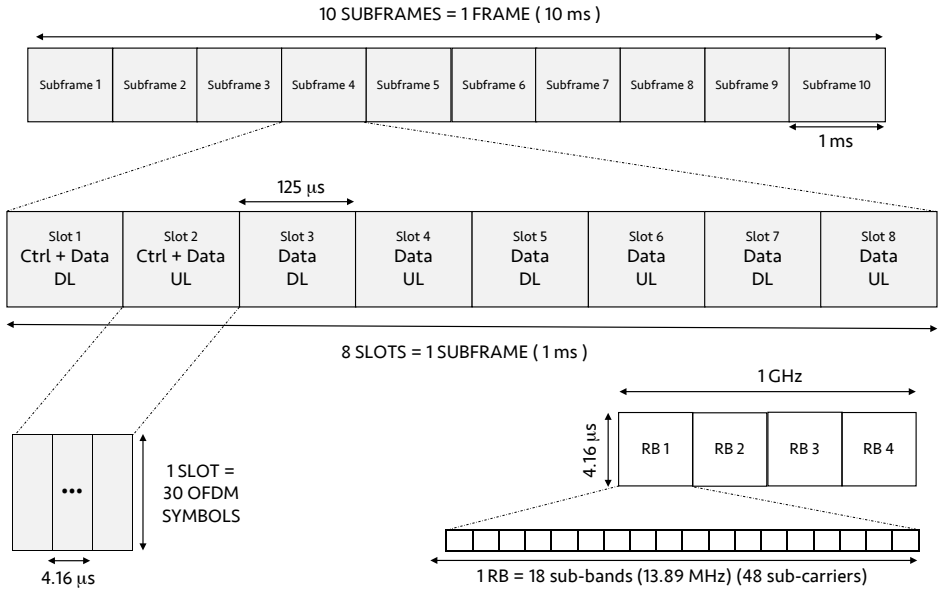

Fig. 4.1: Millimeter-wave NS-3 frame structure.

TIME DOMAIN		
	Number	Duration
Frame	n.d.	10 ms
Subframe	10/frame	1 ms
Slot	8/subframe	125 μs
OFDM Symbol	30/slot	4.16 μs

Table 4.1: Frame structure (time domain).

The choice for the OFDM symbol period relies on the following considerations. For a system implementation with N-point Fast Fourier Transform (FFT) and a subcarrier spacing of Δ_f, the sampling frequency is given by $f_s = N\Delta_f$. The sampling period $T_s = 1/f_s$ gives the symbol period as $T_{\text{sym}} = NT_s$.

In [4], for a 1 GHz bandwidth, the proposed sampling rate is 1106 MHz, with a subcarrier spacing of 270 KHz. Then, there are used:

$$f_s = N\Delta_f \Rightarrow N = \frac{f_s}{\Delta_f} = \frac{1106\,\text{MHz}}{270\,\text{KHz}} = 4096\,\text{points} \tag{4.1}$$

Since $T_s = 1/f_s \simeq 0.904$ ns, the OFDM symbol duration is hence:

$$T_{\text{sym}} = NT_s = 4096 \cdot 0.904\, ns \simeq 3.7\, \mu s \tag{4.2}$$

For small cells, a further guard period of $0.463\,\mu s$ is used, giving a total symbol period of around $3.7 + 0.463 \simeq 4.16\,\mu s$ [33]. Other choices for the OFDM symbol duration can be taken, like the one in [34].

The first two slots are used to control data in DL and UL direction respectively. Slots 3, 5 and 7 are allocated for DL and slots 4, 6 and 8 for UL data transmission. In particular, a switching gap of 1 μs is introduced each time the allocated direction changes from uplink to downlink or vice versa.

In the frequency domain, the entire bandwidth of 1 GHz is divided according to Table 4.2:

FREQUENCY DOMAIN		
	Number	Portion of BW
RB	4/slot	250 MHz
Sub-band	18/RB	13.89 MHz
Sub-carrier	48/sub-band	0.29 MHz

Table 4.2: Frame structure (frequency domain).

Transmission schemes

The *mmWaveEnbPhy* and the *mmWaveUePhy* classes model the physical layer for the BS and the UE respectively.

Broadly the physical layer (i) handles the transmission and reception of signals, (ii) simulates the start and the end of frames, subframes, and slots, (iii) delivers data packets and control messages received over the channel to the MAC layer, (iv) models the decoding error for the received signal and calculate the metrics like the Signal to Interference and Noise Ratio (SINR) and RSRP.

The physical layer contains one instance of the *mmWaveSpectrumPhy* class. The transmission procedure for data frames is performed by the

StartTxDataFrames method. For control messages, *StartTxControlFrames* is instead invoked. The reception procedure is performed by *StartRx* method. The functionality of *StartRx* is further subdivided into *StartRxData* and *StartRxControl*, according to the message type.

After the reception of the data packets, the PHY layer calculates SINR and RSRP of the received signal taking into account the MIMO beamforming gains (as we will see see later in this chapter). This is done by the *mmWaveInterference* class.

The physical layer at the user device maps the calculated SINR into a Channel Quality Indicator (CQI) (Section 4.2.3), which is fed back to the base station for the resource allocation. Control signals are assumed to be ideally transmitted.

4.2.2 Physical (PHY) Layer - Channel Modeling

In this subsection, we will now describe the transmitting channel, as illustrated in Figure 4.2. It's important to highlight that, in a mmW channel, the use of a multi-antenna approach is implemented to perform beamforming, in order to increase the gain, which is particularly critical in millimeter-wave communication.

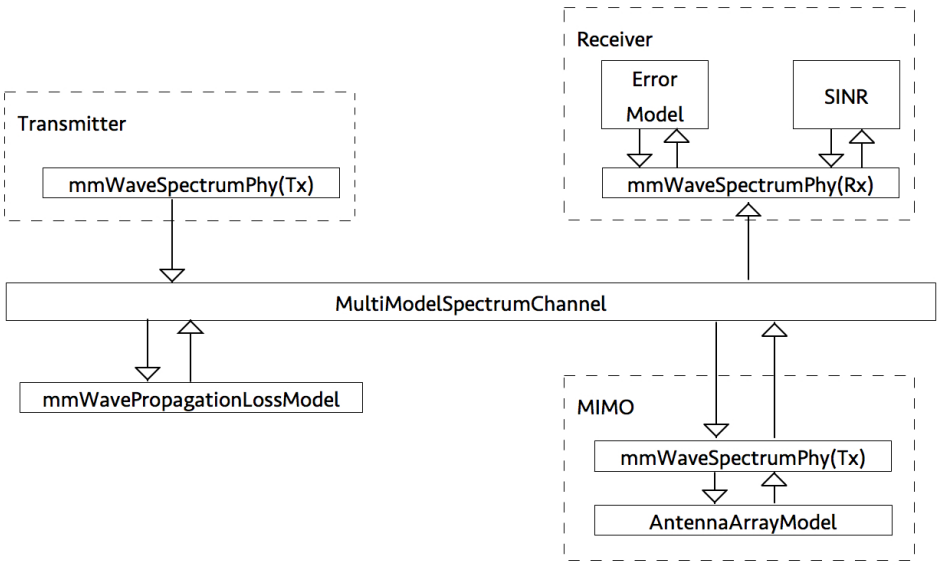

Fig. 4.2: Millimeter-wave channel model.

The link budget for the mm-wave propagation channel has been estimated in [6] as:

$$P_{RX} = P_{TX} + G_{BF} - PL - SW \tag{4.3}$$

where P_{RX} is the total received power expressed in dBm, P_{TX} is the transmit power, G_{BF} is the gain obtained using BF techniques, and PL and SW represent the pathloss and shadowing, respectively.

Propagation Loss Model

The mmW modules work in three different states of pathloss model, depending on the scenario we are working on. These possible states are: LoS, NLoS and outage.

For every link, the code determines the channel state through the following procedure. Based on the distance between the two nodes of the link (transmitter and receiver), the probability to be in one of the states (respectively P_{LoS}, P_{NLoS}, P_{out}) is computed picking a random number P_{ref} in the interval $[0, 1]$ and comparing it with the probability associated to each channel state. In particular, if $P_{\text{ref}} < P_{\text{LoS}}$, the channel will be in a LoS configuration, else if $P_{\text{LoS}} < P_{\text{ref}} < (P_{\text{LoS}} + P_{\text{NLoS}})$ the configuration will be NLoS. Otherwise, it will be outage.

Figure 4.3 (from [6]) shows the fractions of points that were observed to be in each of the three states, depending on the distance between transmitter and received, together with the probability functions $P_{\text{LoS}}(d)$, $P_{\text{NLoS}}(d)$ and $P_{\text{outage}}(d)$ that had been mathematically estimated.

It can be seen that, when we are very close to the BS, the probability to be in LoS is very high while, leaving the transmitter, it is increasingly likely to be in NLoS or even outage [3]. In NS-3, when at the beginning of a simulation it is evaluated the probability to be in one of the three states, if NLoS or outage are picked, a negative offset is considered in the computation of the SINR, in order to take into account the bad mmW channel propagation conditions.

[3] In a urban environment like the one where measurements in [6] had been conducted, the further from the BS, the more likely to have buildings in the path, and so to be in NLoS scenarios.

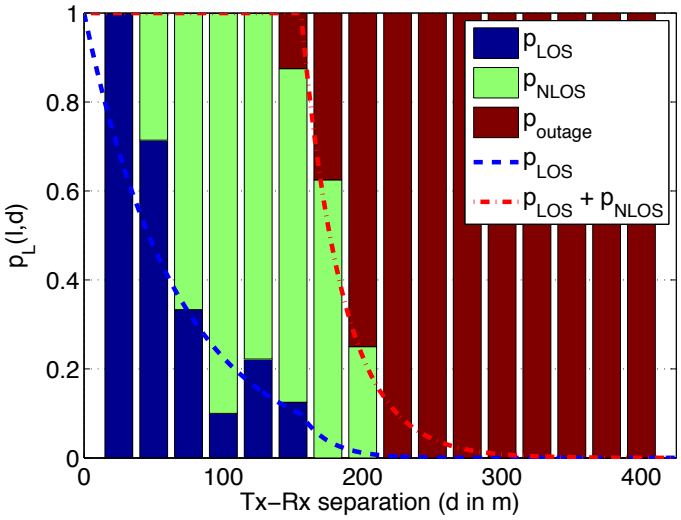

Fig. 4.3: The fitted curves and the empirical values of $P_{\text{LoS}}(d)$, $P_{\text{NLoS}}(d)$ and $P_{\text{outage}}(d)$, as a function of the distance TX-RX d. Figure from [6].

After this initial setting of the channel, the pathloss and shadowing are obtained by:

$$PL(d)[dB] = \alpha + \beta 10 \log_{10}(d) + \xi \tag{4.4}$$

where $\xi \sim N(0, \sigma^2)$ represents the shadowing, d is the distance between receiver and transmitter, while the value of the parameters α, β and σ are given by [6], for each scenario, as reported in Table 4.3:

	28 **GHz**			73 **GHz**		
	α	β	σ [dB]	α	β	σ [dB]
NLOS	72	2.92	8.7	86.6	2.45	8
LOS	61.4	2	5.8	69.8	2	5.8

Table 4.3: Parameters α, β and σ in the case of NLOS or LOS for two frequencies: 28 and 73 GHz. Table from [6].

These parameters have been computed only for the two frequencies of 28 and 73 GHz, which are thus the only two usable in the simulations; more evaluation will be necessary in order to have information about the losses for all the possible frequencies in millimeter-wave range.

Channel matrix

Based on [7], the code models the mmW channel as a combination of a random number $N \sim \max\{\text{Poission}(\lambda), 1\}$ of *path clusters*, each corresponding to a macro-level scattering path (each cluster is further composed of several subpaths L_k), as in Figure 4.4. After many experiments conducted in [6], it has been set $\lambda = 1.8$ for the 28 GHz band and $\lambda = 1.9$ for the 73 GHz band.

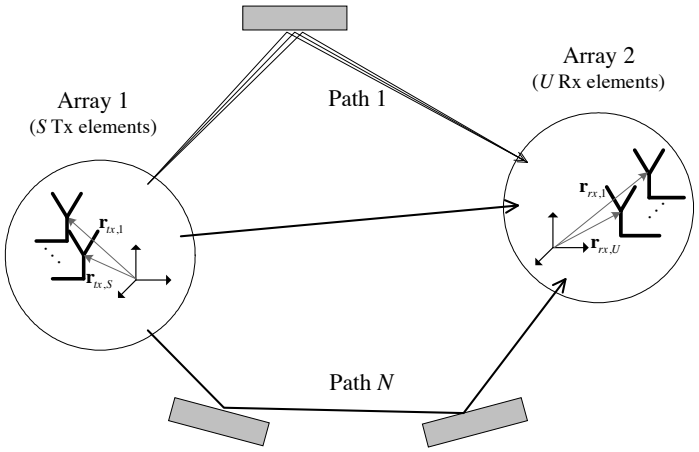

Fig. 4.4: Cluster configuration for the millimeter-wave channel. Figure from [7].

The number N of *path-clusters* is described by the following items.

- A fraction of the total power: for each k^{th} cluster, it is computed in [6].
- Central azimuth (horizontal) and elevation (vertical) Angles of Arrival (AoA)[4] and Angle of Departure (AoD)[5], respectively θ_{kl}^{rx}, ϕ_{kl}^{rx}, θ_{kl}^{tx}, ϕ_{kl}^{tx}.

Thus, the channel matrix is described as follows:

$$H(t,f) = \frac{1}{\sqrt{L}} \sum_{k=1}^{N} \sum_{l=1}^{L_k} g_{kl}(t,f) \mathbf{u}_{rx}(\theta_{kl}^{rx}, \phi_{kl}^{rx}) \mathbf{u}_{tx}^{*}(\theta_{kl}^{tx}, \phi_{kl}^{tx}) \tag{4.5}$$

where $g_{kl}(t,f)$ refers to the small-scale fading over time and frequency on the l^{th} subpath of the k^{th} cluster and $\mathbf{u}_{rx}(\cdot)$, $\mathbf{u}_{tx}(\cdot)$ are the vector response

[4] AoA measurement is a method for determining the direction of propagation of a radio-frequency wave incident on an antenna array.

[5] AoD is the angle of elevation of maximum emission of electromagnetic energy from an antenna.

functions for the receiver and transmitter antenna arrays to the angular arrivals and departures.

The small-scale fading describes the rapid fluctuations of the amplitude of a radio signal over a short period of time or travel distance. It is caused by interference between two or more versions of the transmitted signal which arrive at the receiver at different times. This interference can vary widely in amplitude and phase over time [35]. In equation (4.5), small-scale fading is computed considering the number of clusters, number of subpaths per cluster, Doppler shift, power spread, delay spread and angle or arrival, as given in [6] by:

$$g_{kl}(t,f) = \sqrt{P_{lk}} e^{2\pi i f_d \cos(\omega_k l)t - 2\pi i \tau_{kl} f} \tag{4.6}$$

where P_{kl} is the power spread, f_d is the maximum Doppler shift, ω_{kl} is the AoA of the subpath relative to the direction of motion; τ_{kl} gives the delay spread, and f is the carrier frequency.

During the simulation execution, the small-scale fading is calculated at every slot (this means every 125 μs). In a different manner, for the large-scale fading, the spatial signature matrices are periodically updated every 100 ms, to simulate a sudden change of the channel.

Beamforming

As already explained before, due to high pathloss, multiple antenna elements with beamforming are essential to provide acceptable range of communication in millimeter-wave systems.

The new mmW modules provide a new *AntennaArrayModel* class that supports phased-array antennas. For both transmitter and receiver, the BF vectors are pre-generated offline using another software (i.e., MATLAB ®) and extracted when needed; then the BF gain from transmitter i to receiver j is given by:

$$G(t,f)_{ij} = |\mathbf{w}^*_{rx_{ij}} \mathbf{H}(t,f)_{ij} \mathbf{w}_{tx_{ij}}|^2 \tag{4.7}$$

where, $\mathbf{H}(t,f)_{ij}$ is the channel matrix of ij^{th} link, $\mathbf{w}_{tx_{ij}}$ is the BF vector of transmitter i, when transmitting to receiver j and $\mathbf{w}_{rx_{ij}}$ is the BF vector of receiver j, when receiving from transmitter i.

Beamforming vectors are chosen according to the specific direction that

links BS and UE. In this manner, exploiting the multiple antenna configuration, a directional beam can be established and the BF gain can be computed. Method *SetSector* of said class *AntennaArrayModel* permits to load the right BF vector, based on the right directional sector in which UE and BS communicate. Given the number of antennas in the system and the desired sector, the method returns the BF vector, of a certain width, to be employed in (4.7).

There exist three different types of beamforming: analog, digital and hybrid. *Analog* BF shapes the output beam with only one RF chain, using phase shifters. This model saves power by using only a single A/D or D/A, but has a small flexibility since the BS can only beamform in one direction at a time [36].

Digital BF provides the highest flexibility in shaping the transmitted beams, however it requires one RF chain per antenna element. This increases the cost and complexity, but permits to see in multiple directions simultaneously.

Hybrid (between digital and analog) BF allows the use of a very large number of antennas with a limited number (K) of RF chains. Employing this configuration, the BS can steer and combine to K users at a time, with the full antenna gain [37].

Beamforming in NS-3

In the NS-3 framework, analog BF is implemented through Uniform Linear Array (ULA) . In ULA, a set of two dimensional antenna arrays is used at both BS and UE. The array can be comprised of 8×8, 4×4 or 2×2 elements. The spacing of the elements is set at $\lambda/2$, where λ is the wavelength. These antenna patterns were chosen following the results in [6] and show to offer excellent system capacity for small cell urban deployment, together with easy packageability (for instance, at 28 GHz, a 4×4 array will have a size of roughly 1.5 cm $\times$1.5 cm).

It must be noticed that there exists a strong correlation between beamwidth, number of antenna elements and BF gain. In Figures 4.5, we can see the variation of beamwidths and gains by varying the number of elements in the ULA (this will be a fundamental concept when simulating the CS procedures).

The more antenna elements in the system, the narrower the beams, the

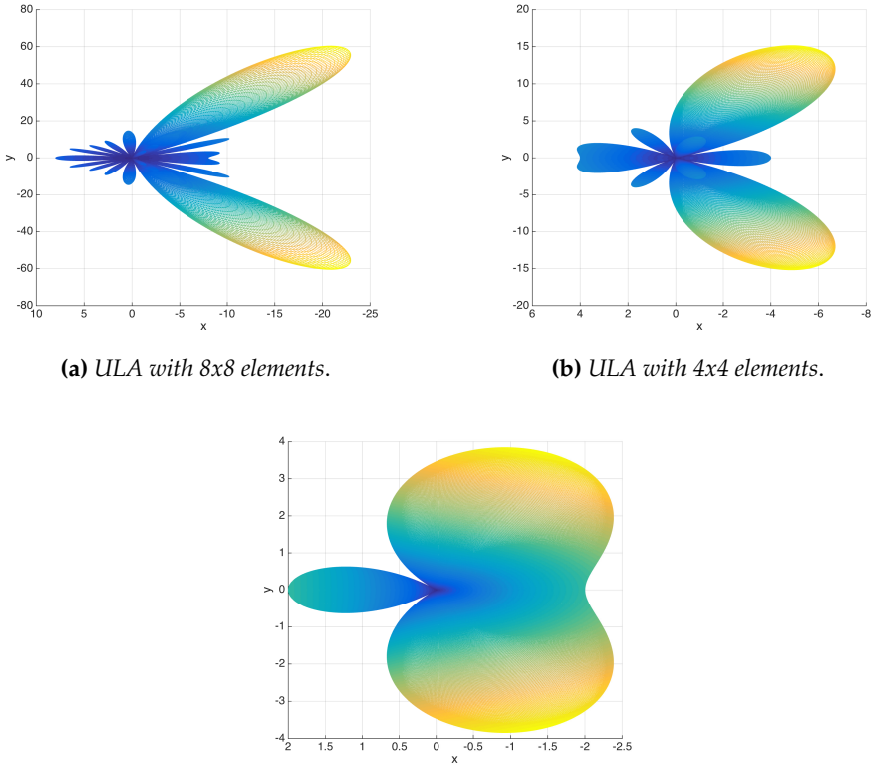

(a) *ULA with 8x8 elements.*

(b) *ULA with 4x4 elements.*

(c) *ULA with 2x2 elements.*

Fig. 4.5: Radiation pattern for ULA. Antenna elements are equally spaced ($\lambda/2$) and the array radiates in direction $\pi/3$ (phase slope of the elements is $\pi/3$). Figures obtained through MATLAB ®.

higher the BF gain, the more precise and directional the transmission. For an 8×8 array, beams can be at most 22.5° wide; for 4×4 system, they are 45° wide; for a 2×2 configuration, beams are 90° wide. Moreover, it can be noticed that this kind of antenna pattern presents some undesired lobes that must be taken into account (for interference purposes) when steering a beam towards a certain direction.

SINR computation

One of the main advantages of the implementation of a directional transmission, when working at millimeter-waves, is that interference is very much lower than in omnidirectional communication. The directionality permits a node to receive a signal only from its transmitter, without almost

any interference from other users, which also exploit a directional communication. However, the computation of the interference is relevant in terms of system level simulation; there might be some special spatial cases where interference is non negligible.

In [31], an interference scheme is proposed, that takes into account the BF directions associated with each link. We have in fact *inter-cell interference* if adjacent BSs are transmitting at the same frequency. Destructive interference is observed when a UE, connected to a certain BS, approaches another BS which transmits at the same carrier frequency.

As we had said before, SINR is computed, at the UE side, after the reception of a data packet. We use Figure 4.6 as a reference, in order to evaluate the SINR between BS_1 and UE_1 in a situation where two BSs are deployed.

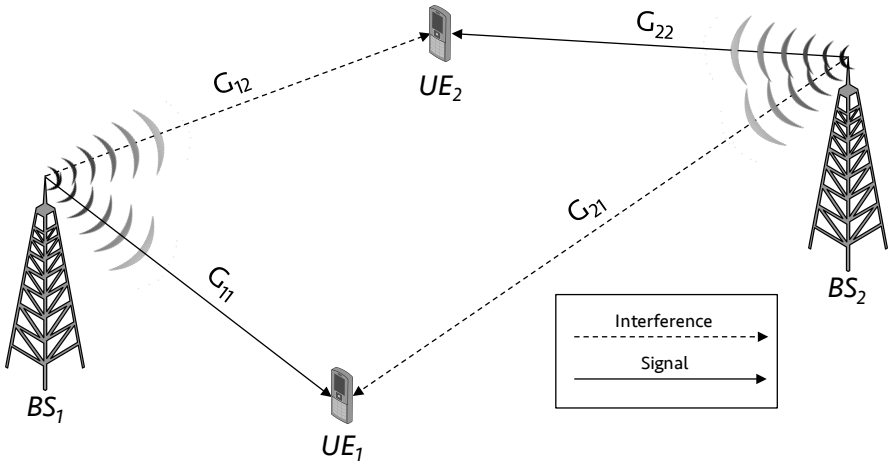

Fig. 4.6: Interference model for SINR computation

First of all, we need to obtain the channel gains associated with both the desired and interfering signals, in order to take them into account when evaluating the SINR. According to equation (4.7), we get:

$$\begin{aligned} G_{11} &= |\mathbf{w}^*_{rx_{11}} \mathbf{H}(t,f)_{11} \mathbf{w}_{tx_{11}}|^2 \\ G_{21} &= |\mathbf{w}^*_{rx_{11}} \mathbf{H}(t,f)_{21} \mathbf{w}_{tx_{22}}|^2 \end{aligned} \tag{4.8}$$

The computation of the $SINR_{11}$ is:

$$SINR_{11} = \frac{\frac{P_{Tx,11}}{PL_{11}} G_{11}}{\frac{P_{Tx,22}}{PL_{21}} G_{21} + BW \times N_0} \tag{4.9}$$

In conclusion, the SINR in this NS-3 framework takes into account:

1. The distance between UE and BS and, in general, the pathloss (which is quite high when working with the mmW frequency band);
2. transmitted powers P_{Tx};
3. interference, when present, and thermal noise $BW \times N_0$;
4. BF gain and directionality, when MIMO is implemented (this contribution may recover the SINR value to acceptable levels);
5. propagation loss model (in NLoS or outage scenarios, a negative offset is considered in the SINR computation, as pointed out in Chapter 4.2.2).

4.2.3 MAC Layer

The MAC layer is developed using the *mmWaveEnbMac* class for the BS and the *mmWaveUeMac* one for the UE. The chief function of this layer is to deliver data packets coming from the upper layers (the net device in this case) to the physical layer and vice versa.

The BS MAC layer is connected to the scheduler module using the MAC-SCHED Service Access Point (SAP) interface, while MAC and PHY are connected through the interface PHY SAP. The relationship between the PHY, MAC and the scheduler module for the BS is depicted in Figure 4.7.

Adaptive Modulation and Coding (AMC)

The scheduler hosts the AMC module. Once, at the UE side, CQI is measured for each downlink data slots that is allocated, the BS scheduler uses this information to compute the most suitable modulation and coding scheme for the communication link.

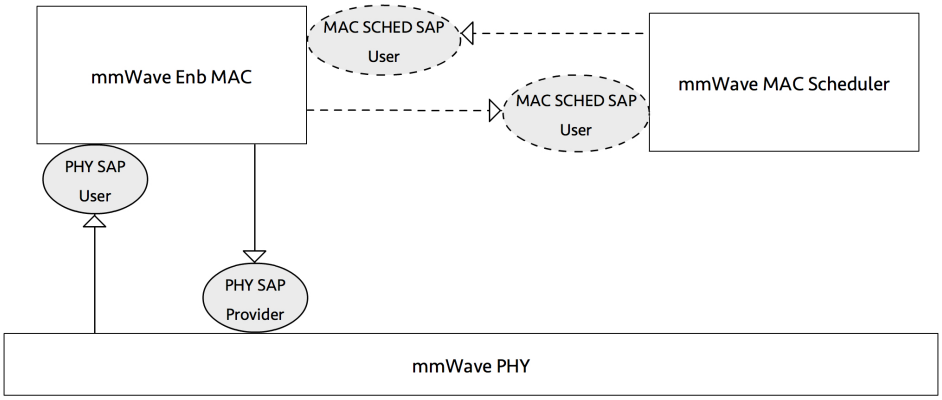

Fig. 4.7: PHY, MAC and scheduler modules with associated SAPs.

During resource allocation, the wide band CQI is used also to determine the Transport Block (TB) size that can be transmitted over the physical layer. It is calculated based on the values of the total number of subcarriers per resource block derived from the user customized configuration, the number of symbols per slot and the number of reference symbols per slot. The higher the CQI value, the higher the size of the TB allocated for that UE.

Scheduler

The virtual class *mmWaveMacScheduler* defines the interface for the implementation of MAC scheduling techniques. The scheduler performs the scheduling and resource allocation for a subframe with both downlink and uplink slots.

Using the *mmWavePhyMacCommon* object, the division of resources in the frequency domain can be customized. The MAC scheduler currently implements a simple Round Robin algorithm to allocate UL and DL data slots to the connected users. All the frequency elements in a particular slot are assigned to the same user, while the control slots are not allocated to any particular user.

Service Access Points

The relationship between modules connected through SAPs can be viewed as that of service providers and users. The SAP provider caters to the re-

quirement of the SAP user based on certain requests received from the user. As in Figure 4.7, there can be identified two different SAPs.

PHY-MAC The communication between the MAC and the PHY layer using the MAC-PHY SAP is through the following processes, as in [31].

1. The subframe indication is sent by the PHY layer to the MAC at the beginning of each slot. The subframe indication for slot 1 for a particular subframe triggers the scheduling procedure for the BS MAC. The subsequent indications are required for upper layer data delivery.

2. The BS MAC maintains data queues for each of the connected UEs and just one such queue is sufficient for the user device. Based on the scheduling scheme and the allocated resources, the MAC layer will send the scheduled number of packets (given by the TB size) to the PHY layer for transmission over the radio link.

3. The scheduling and resource allocation decision received by the BS MAC from the scheduler is relayed to the PHY layer using the *mmWaveResourceAllocation* message. The PHY of the base station in turn transmits this message to all the connected users notifying all the attached devices of the scheduling decision.

4. Based on the SINR of the received data slots, the UE PHY calculates the CQI and transmits it to the base station in the next uplink control slot. The BS PHY on receiving the *mmWaveCqiReport* control message, relays it to the MAC.

MAC-SCHED The eNodeB MAC uses the service provided by the scheduler by the following processes, according to [31].

1. On receiving the subframe indication for slot 1 of a particular subframe, the MAC sends a Scheduling Trigger Request to the scheduler, which returns the scheduling and allocation decisions in the Scheduling Configuration Indication in response to the trigger.

2. The BS MAC, on receiving the CQI information from the PHY, sends it to the scheduler, for future scheduling decisions.

4.3 Simulations in NS-3

When running simulations via NS-3, the following steps are performed:

- a *mmWaveHelper* object is created and initialized;
- node containers for UEs and BSs are created;
- a *ListPositionAllocator* object is created, in order to allocate and deploy users and base stations;
- mobility model is set, for each node in the network;
- a propagation loss model (if different from the default one in [6]), is loaded;
- nodes are finally installed in the cells;
- through method *RegisterToClosestEnb*, each UE is attached to the closest BS in the network;
- a *DataRadioBearer* is activated, so each UE will have data to transmit, during the simulation;
- *Simulator::Stop* programs the simulation duration, while *Simulator::Run* actually starts the script.

In Chapter 6, there are summarised all the parameters we have set, in order to simulate the CS techniques.

Chapter 5

Cell-Search for 5G systems

Papers and works on millimeter-waves and, in particular, referred to procedures like synchronization or Cell-Search are very recent, since research in this field is just at the dawn.

At the beginning of this Chapter, we report some of the most important contributions that have been made up to now, while in the second part we propose different theoretical CS procedures that can be implemented in NS-3 (through modifications of some basic modules), in order to simulate their performance. We assume analog beamforming.

5.1 State of the art

In [25], a two-step procedure is proposed to perform Initial Access (IA). As a first step, the macrocell BS broadcasts synchronisation signals over omnidirectional microwave control channel while, in the second step, the microcell BS performs periodic spatial search using a sequence of pilot transmissions at mmW frequencies, in semi or fully directional mode (this last one is preferred at the expense of higher time required to perform spatial search).

A similar analysis is proposed in [38]. In order to find a new way to perform IA and CS, a comparison between omnidirectional and directional transmission over random directions is presented. Simulations have shown that omnidirectional performs better in terms of time and detection quality. The reason for the degradation when randomly scanning the area is that

the beams often miss the UE and the UE sees very little signal energy.

In [39], the authors propose an exhaustive method that performs directional communication over mmW frequencies. Multiple preamble sequences are sent directionally through narrow beams over multiple directions, in order to cover all the 360° area. The result of this approach is that the growth of the number of antenna elements at either the transmitter or the receiver provides a large performance gain compared to the case of an omnidirectional antenna. However this solution leads to a long duration of the Random Access, with respect to LTE.

In [40], after proposing a CS strategy similar to that in [39], a hierarchical procedure is presented. At the beginning, signals are sent in few directions over wide beams; then, iteratively, the research is refined, using narrower beams, over the best direction found in the previous steps, until communication is sufficiently directional. Simulations show that this search can provide fast discovery but performs worse than exhaustive CS: a UE would more likely select an incorrect beam in the first stage of the hierarchical search and then fail to find a beam with sufficient SINR in the successive stages.

Similarly, in [41] an innovative method is presented. At the first step, training frames are sent through each transmit beam direction sequentially (to cover the whole space), while the UE is set to receive them omnidirectionally. The signal strength from each transmit beam direction is estimated and ranked. In the second phase, this information is fed back to the transmitter, which determines its best direction. At the third and last stage, the BS sends its messages through this best direction and this time the UE scans all the space to determine the best receive beam direction. With this solution, training time is kept short at the expense of losing the beamforming gain, due to the omnidirectional reception in phase one.

Finally, in [24] and [42], new approaches are presented, based on anchor-booster heterogeneous networks, in which booster cells (operating at mmW) are deployed under the coverage of an anchor cell (operating at microwaves). In one solution, the anchor BS gets control over CS, informing the booster

BS about the UE's location, so that the BS can directly steer its antenna array towards the UE's arriving direction (which is known), establishing a reliable directional communication. Results show that this approach requires accurate and expensive algorithms to get reliable location information, but permits to massively reduce the CS time since it is no longer necessary to scan the whole space, in order the find a UE's position.

In conclusion, all the described algorithms present pros and cons, and all of them require further research to overcome their issues and drawbacks. Summarizing, it can be worthy to study and compare the performance of three main strategies: CS based of preliminary exchange of state information, exploiting the concept of heterogeneous cell, CS in which both omnidirectional and directional transmission are used, CS where millimeter-waves are exploited from the very beginning of the procedure. In the next section, we will study this last solution, providing algorithms that can be simulated via NS-3.

5.2 Cell-Search and NS-3 implementation

CS aims mainly at determining the best beam the BS has to set, in order to directly connect to each UE in the cell, and the best beam each UE has to set, in order to directly communicate with the BS.

In this section, we will describe in detail two CS procedures and we will compare them in terms both of *discovery time* (DT) and *miss-detection probability* (P_{MD}). The former refers to the time a BS needs to identify users, the latter to the probability that a UE is not correctly detected, despite being placed within the cell edges. We will also explicitly refer to the NS-3 framework, describing which modifications we have implemented, in order to simulate the two CS models.

UEs compute SINRs only when data is received. Since PSSs are control messages, we have added the possibility to evaluate SINR also for these kinds of received packets, creating *interferenceControl* and *controlChunkProcessor* objects in *mmWaveInterference* class and configuring them in the *Helper* and *mmWaveSpectrumPhy*.

In the code, the two main classes we modify are *mmWaveEnbPhy* and *mmWaveUePhy*. The former, referred to the BS, controls PSS transmissions

and, in the end, chooses the best beam to reach each UE, on the basis of the received information. The latter, referred to the user, controls the reception of PSS messages and deals with the transmission of information control packets that will be collected at the BS side to make beam decisions. It also takes care of finding the best sector to directionally communicate with the BS.

In Figure 5.1, we report the diagram for the portion of the NS-3 framework referred to the implementation of the CS procedure, including the modification we have made to the modules. In the next subsections, each method will be examined in detail. In particular, we will focus on two main CS techniques: (i) *Exhaustive Cell-Search*, Section 5.2.1, (ii) *Iterative Cell-Search*, Section 5.2.2.

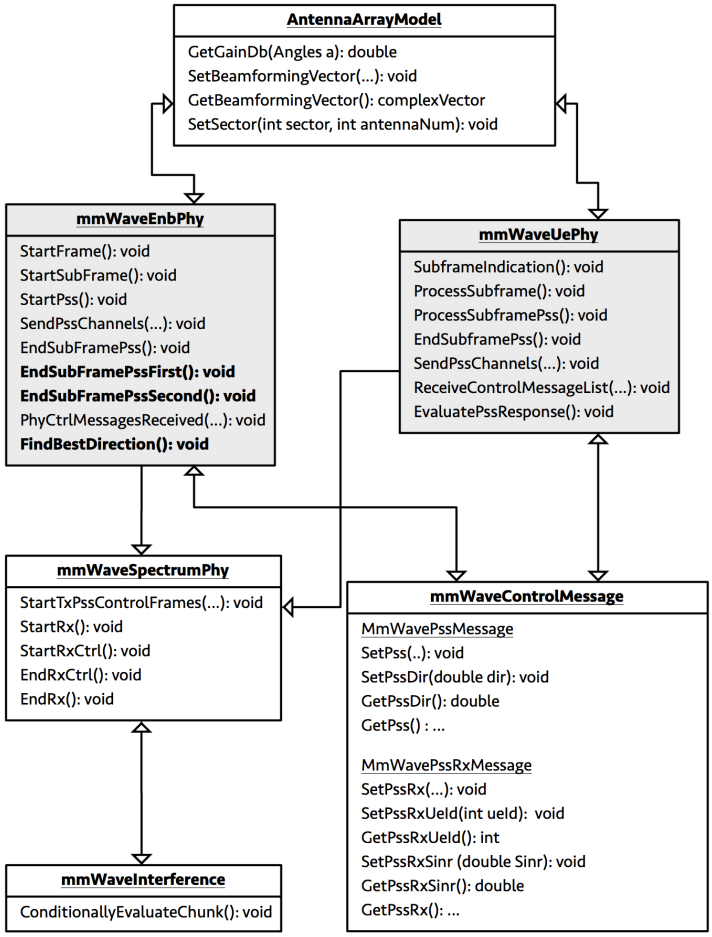

Fig. 5.1: Class diagram of the mmW module, for CS procedure. Methods in bold are referred uniquely to the iterative procedure of Section 5.2.2.

5.2.1 Exhaustive technique

First of all, we present a CS algorithm we will refer to as *exhaustive technique*.

Briefly, the BS sends PSS messages in N directions, in different slots, through narrow beams, while the UE configures its antenna array in order to receive said messages. Upon the reception of a PSS, the UE evaluates the SINR and feeds it back to the BS through a PSS_{RX} message.

After having scanned the all 360° space and having received PSS_{RX} from all reachable users, the BS determines the best beam to directionally reach the UE, on the basis of the higher received SINR (which corresponds to a certain direction). From now on, this UE will be always served through the identified beam. In the meanwhile, at the UE side, the best direction is similarly computed, in order to reach the BS.

Figure 5.2 represents the exhaustive CS technique at the BS side, where one beam at a time is sent.

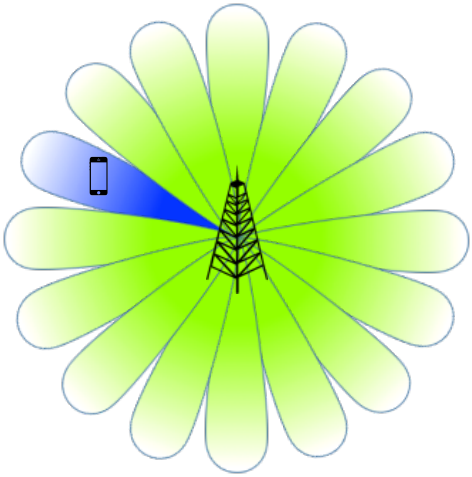

Fig. 5.2: Exhaustive Cell-Search technique at BS side.

Exhaustive CS: frame structure

As a design choice, the BS is equipped with 64 (8×8) antennas and can steer beams which have a 22.5° width. The UE has a 4×4 antenna array and can steer 45° width beams.

Each CS slot has a duration of around 100 μs, which is sufficiently small to ensure a coherent channel even at the very high mmW frequencies [33]. Moreover, in [43], it is said that beam switching time from one sector to

another takes around 100 ns, which is much less than 100 μs and so can be neglected. In particular, since in Chapter 4 we have designed an OFDM symbol to have length 4.16 μs, we assign 25 OFDM symbols to each CS slot, which thus has length $T = 4.16\,\mu s \cdot 25 = 104\,\mu s$.

The BS will send PSS messages in $N = 16$ directions through $\frac{360^\circ}{16} = 22.5^\circ$ width beams, exploiting its maximum achievable BF gain. The UE has a set of combining vectors that also cover the whole angular space; it will thus receive PSSs through four $\frac{360^\circ}{4} = 90^\circ$ width beams (using a 2×2 antenna pattern) or through eight $\frac{360^\circ}{8} = 45^\circ$ width beams (using all the 16 antenna elements it is equipped with), while it will always transmit its PSS_{RX} through 45° width beams.

Considering a 4-directions reception, the frame is structured as in Figure 5.3. At the BS side, 4 PSS messages are sent in the same direction, in 4 consecutive DL slots, in order to match with one of the 4 reception beams the UE steers. Then, in the UL slot, the user feeds back its PSS_{RX}, which is in turn collected at the BS (in receiving mode). These 4DL and 1UL slots constitute a *CS macroelement*. After the UL slot, the BS starts sending another macroelement block in the next direction, to cover the whole 360° space.

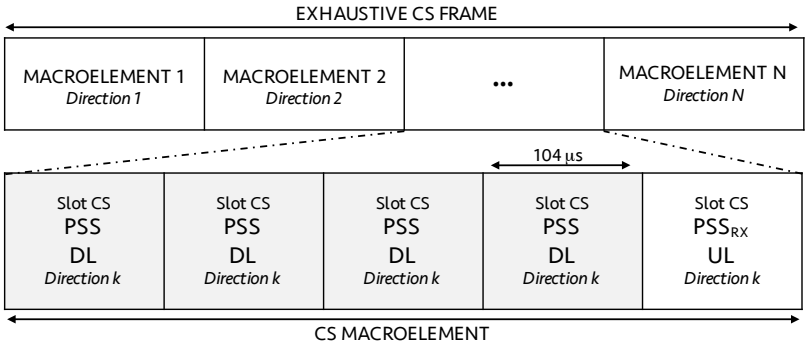

Fig. 5.3: Exhaustive CS frame structure, when UE receives in 4 directions.

Since $N = 16$, 16 CS macroelements are sent, resulting in $16 \cdot 5 = 80$ slots. At the end of this procedure, decisions at both UE and BS sides are made, in order to determine the best beam pair to set up, for directionally communicating.

On the other hand, if the UE is programmed to scan in 8 directions when receiving (45° width, using its full 4×4 antenna pattern), the frame structure is modified and the macroelement is composed of 8 DL slots and 1 UL slot. Then, there will be $16 \cdot 9 = 144$ CS slots. In Chapter 6, we will com-

pare these different solutions in terms of several metrics, such discovery time and miss-detection probability.

Exhaustive CS: NS-3 implementation

In this subsection, we outline in detail the exhaustive technique and the changes we have made to the NS-3 mmW framework.

Let's consider a macroelement k, referred to the direction $k/16$. We want to find the best sector to reach user i. We will dwell on the case where a UE receives in 4 directions (the 8-directions case is its natural extension).

Step 1 At the BS side, method *StartPss* is called and a PSS message is built. A header with the ID of the sector through which the PSS will be sent is added (*SetPssDir*). Then, method *SendPssChannels* permits to actually transmit the PSS. *SetSector* is invoked to configure the antenna array to steer a 22.5° beam towards the selected direction (all the 16 directions will be scanned from time to time).

Step 2 At the UE side, if it is a DL slot, the user configures its antenna towards one out of four (or out of eight) directions, to receive a PSS from the BS. Then method *ProcessSubframePss* is called. The UE extracts from the PSS header the BS sector ID (through method *GetPssDir*). Moreover, SINR is evaluated and finally collected.

Method *EvaluatePssResponse* permits to see if the computed SINR is above a certain threshold. If so, the UE will transmit, in the UL slot in Step 4, a PSS_{RX} message to the BS.

Step 3 At the end of a DL slot (*EndSubFramePss*), the BS evaluates if it has already sent 4 PSS messages in the current direction k, in order to rendezvous with one of the 4 receiving UE beams (or 8 PSSs, if the UE receives in 8 directions). If so, an UL slot occurs. Otherwise, Step 1 is performed again and another PSS is sent in the same direction.

At the UE side, if the user has already scanned the 360° space with four (or eight) beams, in reception mode, then an UL slot occurs. Otherwise, it configures its antenna pattern to receive in the next direction.

Step 4a When the UL slot occurs, UE starts building its PSS_{RX} message (only if it has received at least one PSS with SINR above threshold). The header comprises: (i) information about the current UE ID (*SetPssRxUeId*), (ii) SINR value of a PSS message, evaluated before (*SetPssRxSinr*). If the UE has received multiple PSSs in more than one DL slot, the direction β corresponding to the maximum evaluated SINR will be chosen. Without any other analysis, this direction could be the right one to steer back the PSS response.

If now the UE wants to respond with a narrow beam (45° width, exploiting its 4×4 antenna array), it needs to know the direction precisely. In order to do this, there are at least the following possibilities:

1. if UE and BS share an absolute angular reference, the direction can be mathematically found, on the basis of the beam ID the BS has embedded in its PSS message (and that UE has extracted in Step 2)[1].

2. UE receiving in 90° sectors can perform AoA estimation algorithms. There are lots of papers and works on the subject, like [44–47]. In this way, the user can estimate the arrival direction and configure its antennas to steer a message towards that direction. This is actually implementable only because the receiving beam is wider than the transmitting one;

3. if the UE searches at finer resolution, receiving in 8 directions, the best receiving direction found (corresponding to the maximum SINR) can be immediately set as response beam[2].

Therefore, after having determined the right 45° direction $\tilde{\beta}$ (through one of the proposed solutions), a *UeSectorMap* is created, as:

$$\text{Sector } \tilde{\beta} \Longleftrightarrow SINR_{\tilde{\beta}}$$

In such a way, the UE knows that the BS can be reached, through sector $\tilde{\beta}$, achieving an SINR equals to $\text{SINR}_{\tilde{\beta}}$. Finally, *SetSector* is invoked to con-

[1] In NS-3, we assume that an estimation technique is performed but, in a real-environment simulation, more sophisticated solutions must be implemented. We reserve this analysis as a future work.

[2] This solution is feasible but at the expense of a longer search time, since now the BS has to examine more combinations, in order to match with one of the UE receiving beams.

figure the antenna pattern towards direction $\tilde{\beta}$. Method *SendPssChannels* allows to actually perform the transmission.

Step 4b On the other side, the BS expects to receive a PSS_{RX} message. The reception beam is steered in the same direction of the previous four DL slots. If PSS_{RX} is detected, there are extracted its embedded information. In particular, it is saved the SINR (*GetPssRxSinr*) evaluated by UE having ID i (obtained through method *GetPssRxUeId*), and referred to one of the PSSs sent in a DL slots. A *BsSectorMap* is created, as:

$$\text{Sector } k \iff \text{UE } i \iff SINR_{k,i}$$

In such a way, the BS knows that, if a beam is steered towards direction k to reach UE i, this SINR will be $\text{SINR}_{k,i}$. If no PSS_{RX} is received, it means that no UEs are detected in direction k (at least no UEs having a SINR above threshold).

Step 5 After the UL slot, the UEs returns to the reception mode, restarting the 4 (or 8) directions scan, looking for new PSSs. On the other hand, the BS configures its antenna elements in order to steer beams to the next direction $k+1$, up to cover the whole 360° space. Step 1 is cyclically performed again, *UeSectorMap* and *BsSectorMap* are updated with new entries.

Step 6 When all the 16 directions will be scanned by the BS, the CS procedure ends, followed by the decision phase.

Decision phase In this phase, both UEs and BS select the best beam to reach each other, from now on. The user enters its *UeSectorMap* looking for the maximum SINR value saved. The corresponding direction in the map is the right one to set, when it will have to send messages to the BS.

Similarly, the BS enters its *BsSectorMap* and, for each UE ID, it will find the sector corresponding to the higher SINR saved. This beam will be chosen to reach that UE.

Algorithm 1 shows the exhaustive technique's steps at the BS side.

Algorithm 1 Exhaustive technique at BS side

```
1: procedure EXHAUSTIVEBS(16, 4)                    ▷ 16 transmitting and 4 receiving directions
2:     if numDL=4 && prevSlot=DL then                ▷ The UE has scanned the whole angular space
3:         nextSlot=UL; StartPss();
4:     else if prevSlot=UL then                      ▷ Just received PSS_RX message
5:         sectorPss++;                              ▷ Send PSS in next direction
6:         nextSlot=DL; numDL=0; StartPss();
7:     else if numDL< 4 then                         ▷ UE still has to scan around
8:         numDL++;        ▷ Again in the same direction to rendezvous with UE (another DL slot)
9:         StartPss();
10:    else                                          ▷ Covered all 360° space
11:        CS=false; StartSubFrame();                ▷ End of CS procedure
12:    end if
13: end procedure
```

Algorithm 2 shows the steps of the exhaustive procedure at the UE side, when user receives in 4 directions (the 8-directions case is similarly obtained sending 8 DL slots before an UL one).

Algorithm 2 Exhaustive technique at UE side

```
1: procedure EXHAUSTIVEUE(16, 4)                    ▷ 16 transmitting and 4 receiving directions
2:     if numDL=4 && prevSlot=DL then                ▷ The UE has scanned the whole angular space
3:         nextSlot=UL; SubframeIndication();
4:     else if prevSlot=UL then                      ▷ Just transmitted PSS_RX message
5:         sectorPss=0;                              ▷ Restart the scan for a new BS direction
6:         nextSlot=DL; numDL=0; SubframeIndication();
7:     else if numDL< 4 then                         ▷ UE still has to scan around (another DL slot)
8:         numDL++;
9:         sectorPss++;                              ▷ Receive PSS in the next direction
10:        SubframeIndication();
11:    else                          ▷ BS has covered all 360° space and no more PSS to receive
12:        CS=false; SubframeIndication();           ▷ End of CS procedure
13:    end if
14: end procedure
```

5.2.2 Iterative technique

In this section, we present another CS algorithm we will refer to as *iterative technique*. Briefly, the procedure is structured into two main phases.

In the first phase, as shown in Figure 5.4(a), the BS sends PSS messages in 4 macro directions, in different slots, through wide beams, while the UE configures its antenna array in order to receive said messages. Upon the reception of a PSS, the UE evaluates the SINR and feeds it back to the BS through a PSS_{RX} message. After having scanned all the 360° space, the BS determines the best beam (out of four), on the basis of the higher received SINR (and similarly the UE finds the best direction to reach the BS).

In the second phase, like in Figure 5.4(b), the BS refines its search only in the previously identified best direction. Then, four narrow beams are sent up to cover this 90° macro sector, while the UE receives through its own best direction. Finally, other PSS_{RX} messages are sent towards the BS, in order to determine, through another SINR analysis, a more precise beam to directionally reach the UE.

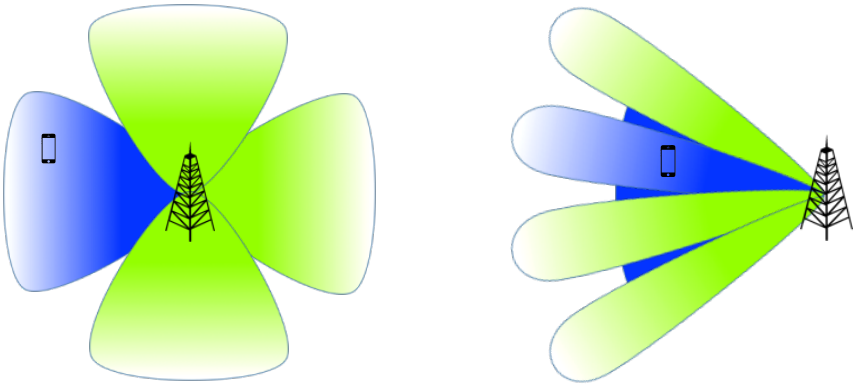

(a) *Phase 1.* **(b)** *Phase 2.*

Fig. 5.4: Iterative CS technique at BS side.

Iterative CS: frame structure

As for the exhaustive technique, BS and UEs are respectively equipped with 64 and 16 antenna elements. Each CS slot is composed of 25 OFDM symbols and has a length of 104 μs. In the first phase, the BS will send PSS messages in $N_1 = 4$ macro directions through four 90° beams and the UE can receive in either 4 or 8 directions, covering the whole angular space. In the second phase, instead, the BS will send the refining PSSs through $N_2 = 4$ narrow 22.5° beams, while the UE will configure its antenna array to receive only in its best direction (previously identified).

If the UE is programmed to receive in 4 directions, in the first phase, the frame is structured as in Figure 5.5.

As for the exhaustive procedure, in the first phase, a CS macroelement is constituted of four DL slots (for the 4 PSSs sent in the same direction, to match with one UE receiving beam) and one UL slot, reserved for the PSS_{RX}. Since four macroelements are sent in the four 90° directions, we

have $5 \cdot 4 = 20$ slots. In the second phase, after having determined the best macro direction k of the previous stage, four other macroelements are transmitted, to refine this sector through narrow beams. This time, each macroelement is composed of only 1 DL slot for the PSS and 1 UL slot for the PSS_{RX}, since now the UE no longer needs to scan in reception. Then, $2 \cdot 4 = 8$ slots are sent. On the whole, the search needs $20 + 8 = 28$ slots to be performed.

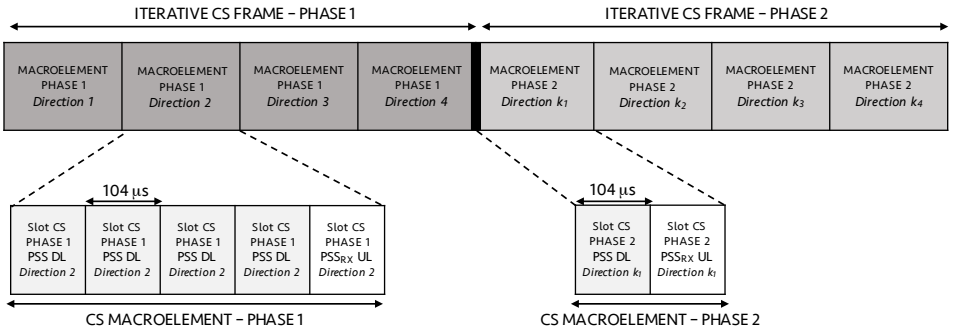

Fig. 5.5: Iterative CS frame structure, when UE receives in 4 directions, in the first phase.

On the other hand, if the UE scans in 8 directions, the frame structure of Figure 5.5 is slightly modified. There will be needed 8 DL and 1UL slots and so $9 \cdot 4 = 36$ slots in the first phase, while the usual 8 for the second stage, for a total of $36 + 8 = 44$ CS slots.

Iterative CS: NS-3 implementation

In this subsection, we describe in detail the iterative technique and the modifications we have made to the NS-3 mmW framework. We will dwell on the case where a UE receives in 4 directions (the 8-directions case is its natural extension), referring also to some similarities with the exhaustive technique of Section 5.2.1.

First phase - Step 1 At the BS side, method *StartPss* is called and a PSS message is built, as in the exhaustive algorithm. This time, *SetSector* is invoked to configure the antenna array to steer a 90° beam towards the selected macro direction. In the meanwhile, the UE configures its antenna towards one out of four (or out of eight) directions, to receive a PSS from the BS; SINR is computed and the usual *EvaluatePssResponse* method is called.

First phase - Step 2 At the end of a DL slot (*EndSubFramePssFirst*), if the BS has already sent 4 PSS messages (or 8, if the UE receives in 8 directions) in the current macro sector, an UL slot occurs. Otherwise, the BS will send another PSS through the same beam and the UE will receive in its next direction.

First phase - Step 3 In the UL slot, the UE sends its PSS_{RX} message to the BS. There are the following possibilities:

1. if the UE receives in 4 directions, it has to send back its PSS_{RX} through one out of four 90° width beams. In fact, differently from the exhaustive search, no AoA estimation can be performed, since the receiving beam is not wider than the transmitting one. This implies that the UE cannot exploit its maximum BF gain, even after the CS procedure;

2. if the UE receives in 8 directions, at the expenses of a higher discovery delay, the response beam coincides with the best receiving direction found (corresponding to the maximum SINR), and so the user can send its PSS_{RX} through one out of eight 45° width beam, exploiting all its 4×4 array.

The BS, in turn, will collect the information embedded in the PSS_{RX} message.

First phase - Step 4 After the UL slot, the BS starts sending PSSs through the next macro sector, up to cover the whole angular space, and Step 1 is cyclically repeated.

At the end, user enters its *UeSectorMap* and finds the best direction γ to reach the BS, based on the maximum SINR saved. Similarly, the BS accedes its *BsSectorMap* and, for each UE ID, it finds the macro sector k corresponding to the higher SINR saved: this beam is the one that will be refined, in the next phase. Method *FindBestDirection* is called to determine the four 22.5° directions k_1, k_2, k_3, k_4, within that macro sector, that will be investigated.

Second phase - Step 1 At the BS side, another PSS message is steered towards the direction k_i, $i = 1, \ldots, 4$. In the meanwhile, the UE configures its antenna towards its best direction γ. It follows an UL slot (*EndSubFramePssSecond*).

Second phase - Step 2 In the UL slot, the UE sends through beam γ a PSS_{RX} message with the usual fields, that will be collected at the BS side. Then the *BsSectorMap* is updated, in order to take care of this refining information.

Second phase - Step 3 After the UL slot, UE returns in reception mode and BS inspects the next direction k_{i+1}, up to scan the whole 90° macro sector k. Finally, the last decision phase occurs, before concluding the CS procedure.

Decision phase In this stage, the BS selects the best beam to reach each user, from now on, while UE already knows its best direction γ from the first phase of the iterative technique. Therefore, the BS enters again its *BsSectorMap* and, for each UE ID, it finds the sector (now a 22.5° width beam) corresponding to the higher SINR saved. At this time, both BS and UEs know how to directionally reach each other, in the best possible way.

Algorithm 3 shows the steps of the iterative technique at the BS side. First phase refers to Algortithm 1, when BS transmits through 4 macro directions.

Algorithm 3 Iterative technique at BS side

```
1: procedure ITERATIVEFIRSTPHASEBS(4, 4)   ▷ 4 transmitting 90° directions, 4 receiving directions
2:     if # macroelemts < 4 then   ▷ The BS still has to scan the whole angular space
3:         same steps of Algortithm 1 through 90° beams
4:     else   ▷ Covered all 360° space with four wide beams
5:         firstPhase=false; StartSubFrame();   ▷ End of first phase of CS procedure
6:         IterativeFirstPhaseBS(4,4);   ▷ Start second phase
7:     end if
8: end procedure
9:
10: procedure ITERATIVESECONDPHASEBS(4, 4)   ▷ 4 transmitting 22.5° directions, 4 rx directions
11:     FindBestDirection   ▷ Evaluate the four narrow beams to refine the best sector of first phase
12:     if DLslot then   ▷ It is a DL slot, the BS sends a PSS
13:         nextSlot=UL; StartPss();
14:     else if ULslot then   ▷ Just received PSS_RX message
15:         sectorPss++;   ▷ Send PSS in the next direction
16:         nextSlot=DL; StartPss();
17:     else   ▷ BS has covered all 90° macro sector area
18:         CS=false; StartSubFrame();   ▷ End of CS procedure
19:     end if
20: end procedure
```

Algorithm 4 shows the steps of the iterative procedure at the UE side when user receives in 4 directions, in the first phase (the 8-directions case is similarly obtained sending 8 DL slots before an UL one).

Algorithm 4 Iterative technique at UE side

```
1: procedure ITERATIVEFIRSTPHASEUE(4, 4)   ▷ 4 transmitting 90° directions, 4 receiving directions
2:     if # macroelemts < 4 then           ▷ The BS still has to scan the whole angular space
3:         same steps of Algortithm 2
4:     else                                ▷ BS has covered all 360° space with wide beams
5:         firstPhase=false; SubFrameIndication();   ▷ End of first phase of CS procedure
6:         IterativeFirstPhaseUE(4,4);               ▷ Start second phase
7:     end if
8: end procedure
9:
10: procedure ITERATIVESECONDPHASEUE(4, 4)   ▷ 4 transmitting 22.5° directions, 4 rx directions
11:     FindBestDirection                   ▷ Evaluate best direction γ to communicate with the BS
12:     if DLslot then                      ▷ It is a DL slot, the UE receives a PSS through sector γ
13:         nextSlot=UL; StartPss();
14:     else if ULslot then                 ▷ Just transmitted PSS_RX message through sector γ
15:         nextSlot=DL; SubframeIndication();
16:     else                                ▷ BS has covered all 90° macro sector area
17:         CS=false; SubframeIndication();           ▷ End of CS procedure
18:     end if
19: end procedure
```

Chapter 6

Simulations and results

6.1 Simulated scenarios

6.1.1 Simulation assumptions

In the simulations we use the NS-3 framework we have described in the previous chapters, but with the following assumptions.

1. We will assume to consider just the 28 GHz case as carrier frequency for the mmW network. In fact, the 73 GHz case (the only other frequency for which we have some real-environment measurements available) presents worse propagation characteristic (due to the higher frequency) and will be analysed in future works.
2. will assume a static deployment, where no users are moving, during the simulation. In such a way, no handover management is required and it is not necessary to track the UE's motion.
3. We will assume to work in a urban environment (i.e., New York City), whose spatial statistical models of [6] is used in this framework.
4. We will assume to always use analog beamforming, when steering directional beams between BSs and UEs.

All the assumptions we have described, in any case, do not affect the performance of the CS procedure we are presenting in this thesis, and can be relaxed or removed, in future works, when the NS-3 framework will have more sophisticated features.

6.1.2 Simulation parameters

The parameters in the simulated scenarios are based on realistic system design considerations and are summarised in Table 6.1.

Parameter	Value	Description
OFDM symbols per slot	25	
OFDM symbol duration	4.16 μs	
CS slot length	104 μs	$25 \cdot 4.16\,\mu s$
BW	1 GHz	Total system bandwidth
DL - UL P_{TX}	30 dBm	Transmission power
NF	5 dB	Noise figure
f_c	28 GHz	Carrier frequency
R	$0 \div 200$ m	Cell radius
τ	-10, -5, 0 dB	SINR threshold
BS antenna	8×8 ULA	
UE antenna	4×4 ULA	
SimTime	20 ms	Simulation time
Number of repetitions	2000	Montecarlo evaluation
BS position	$(0, 0, 0)$ m	
UE position	varied	Uniform in annulus
UE speed	0 m/s	No mobility
BF	analog	Beamforming architecture
Propagation loss model	LoS, NLoS, outage	Refer to Figure 4.3

Table 6.1: Simulation parameters for CS procedure.

The transmission power P_{TX} for both UL and DL is set to 30 dBm. In fact, in [48] , it is said that a typical transmit power for cells within a radio range of 300 m is from 23 to 30 dBm. Noise figure, which refers to the loss in the SINR due to non-idealities in the receiver, is set to 5 dB.

A typical 5G cell is envisioned to have a radius of around $100 \div 200$ m, accordingly to the channel characteristics [49]. Moreover, from Figure 4.3 and implementing the mmW channel described in [6], we can see that probabilities of NLoS or outage are very high even around 100 m, and so we expect to consider very small cell radii.

Referring to the CS procedures, we will consider three different SINR thresholds τ: -10, -5 and 0 dB. If the SINR is below τ, it is assumed that the UE does not receive any PSS signal. In [40], the threshold is set to -4 dB. Reduction of τ permits to find more users, at the cost of designing more complex (and expensive) receiving schemes, able to detect more corrupted messages.

Simulations are conducted increasing the distance of the UE from the BS, placed at coordinates $(0, 0, 0)$ m, from 0 to 200 m, with 10 m steps. At each iteration, the user is deployed within an annulus having outer radius R_1 and inner radius R_2, with $R_2 < R_1$, according to a uniform distribution. In order to make reliable measurements, through a Montecarlo estimation, each simulation is repeated 2000 times, considering different seeds.

Miss-detection probability is computed in the following way: (i) a user is uniformly deployed in the annulus at distance R from the BS; (ii) one of the CS algorithms is performed and, at the end, if the user is not identified (having SINR below threshold), a counter is incremented by one; (iii) at the current distance, steps (i-ii) are cyclically repeated 2000 times, updating the counter. Finally, the probability is computed as:

$$P_{\text{MD}}(R) = \frac{\#\ \textit{times SINR} < \textit{threshold}}{\#\ \textit{repetitions}} = \frac{\textit{counter value}}{2000} \tag{6.1}$$

Then, the procedure is repeated again, for a different distance from the BS, up to cover the whole range from 0 to 200 m.

We will consider different SINR thresholds and different antenna array configurations, according to the reception mode the UE is programmed to be (either 4 or 8 receiving beams).

Another metric that will be plotted is the *average SINR* for the two different CS techniques. In particular: (i) a user is uniformly deployed in the annulus at a certain distance R; (ii) one of the CS algorithms is performed

and, at the end, user SINR is collected, independent of any threshold; (iii) at the current distance, steps (i-ii) are cyclically repeated 2000 times, memorizing all the SINRs. Finally, $\text{SINR}(R) = \mathbb{E}[SINR(1, \ldots, 2000)]$. Then, the procedure is repeated again, for a different distance from the BS, to cover the whole range from 0 to 200 m.

Furthermore, algorithms will be also compared from the *discovery time* point of view, for different implementation choices.

6.2 Figures and results

6.2.1 Discovery time

First of all, we compare the different CS techniques from the discovery time point of view. Referring to Chapter 5, each CS slot has length of 104 μs, then each procedure presents the time performance of Table 6.2:

Procedure	Number of CS slots	Time
Exhaustive 16×4 16 transmit beams 4 receiving beams	80	$80 \cdot 104\,\mu s = 8.32$ ms
Exhaustive 16×8 16 transmit beams 8 receiving beams	144	$144 \cdot 104\,\mu s = 14.976$ ms
Iterative 4×4 4 transmit beams in 1^{st} phase 4 receiving beams	28	$28 \cdot 104\,\mu s = 2.912$ ms
Iterative 4×8 4 transmit beams in 1^{st} phase 4 receiving beams	44	$44 \cdot 104\,\mu s = 4.576$ ms

Table 6.2: Time to implement CS procedure, for different techniques.

We clearly see that iterative techniques outperform the exhaustive ones, in terms of discovery time. In fact, there is no need to scan the whole 360°

angular space, to find the UE, since it is sufficient to only refine a 90° macro sector. On the other hand, exhaustive methods need to steer narrow beams in all the directions.

Moreover, reception through 4 sectors needs fewer slots to be implemented, since there are less combinations the BS has to try, in order to rendezvous with one UE beam, when transmitting PSS messages. This helps to reduce the search time, at the expense of lowering the BF gain, degrading the UE discovery performances.

6.2.2 SINR evaluation

Figure 6.1 plots the average SINR, in dB, of both exhaustive and iterative CS techniques, when UE receives in either 4 or 8 directions, varying the distance between BS and user, from 0 to 200 meters.

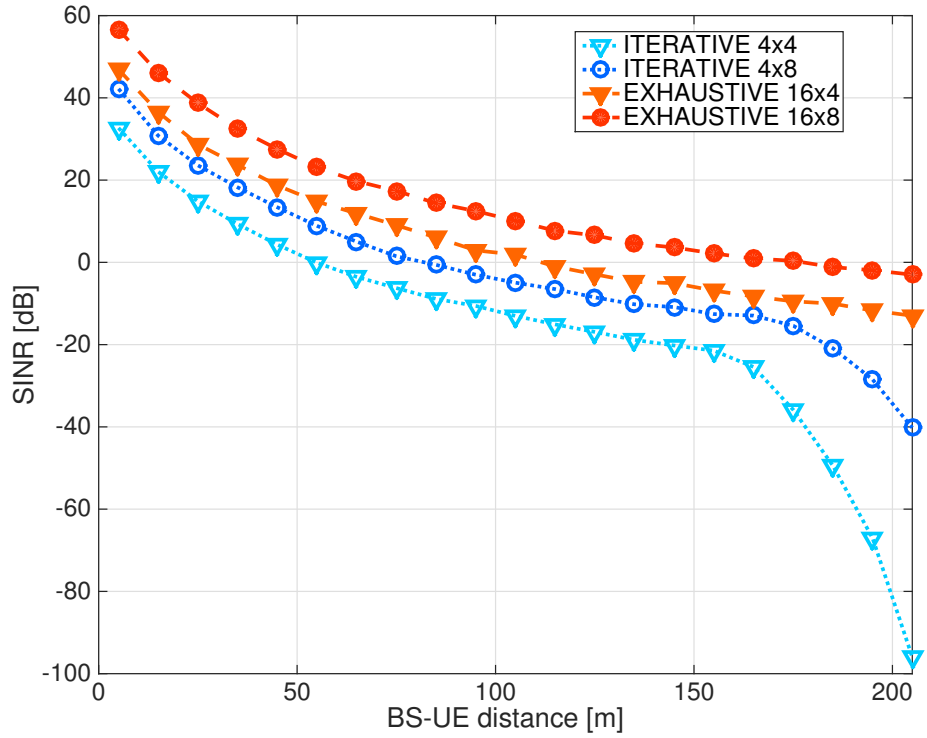

Fig. 6.1: Average SINR for exhaustive and iterative techniques, when UE receives in either 4 or 8 directions, as function of the BS-UE distance.

The following considerations can be made.

SINR shows the expected decreasing behaviour as the distance BS-UE increases. This trend depends both on the pathloss, effect that increases when departing from the BS, and on the NLoS condition (which adds a negative offset to the SINR), whose probability becomes higher moving further from the BS.

The average SINR of the exhaustive technique outperforms that of the iterative procedure. This is due to the BF gain. We have seen in Chapter 4 that, at the same distance, the BF gain (and thus SINR) grows when increasing the number of antenna elements in the communication. Therefore, the iterative algorithms, where BS employs only 4 antennas when transmitting PSSs in the first phase, for discovery time purposes, show worse SINR values than the exhaustive techniques (which use 64 antennas instead), distance being equal.

The performance degrades when UE receives in four 90° directions, since the BF gain is reduced due to wide sectors scan. In fact, this design choice makes use of only 4 antennas in the ULA array, while receiving in eight 45° directions requires instead 16 elements. In conclusion, the *iterative* 4×4 scheme is the worst one, in terms of received SINR, since it exploits only partially the BF gain, while the *exhaustive* 16×8 scheme shows the highest SINR values, employing beams as narrow as possible, at the expense of a longer discovery delay.

It can be noticed that SINR starts rapidly to sink around $160 \div 200$ meters, for the iterative algorithms, while, for lower distances, it showed a smooth decreasing behaviour. This depends on the characteristics of the mmW channel described in [6]. When the distance between BS and UE is above a certain value, with high probability the user would be in outage and an offset of around -300 dB would be added. Since iterative techniques are also affected by low BF gains, this outage condition is already reached around 150 meters, while the exhaustive algorithms still present much higher SINRs. In this way, smaller cell radii must be considered, in order to avoid outage.

Figure 6.2 shows the Cumulative Distribution Function (CDF) of SINR for the four CS configurations presented, when BS and UE are 120 m far. We see that, when for example SINR $= -5$ dB, the gap between the *iterative* 4×4 scheme and the *iterative* 4×8 is much less than the gap between

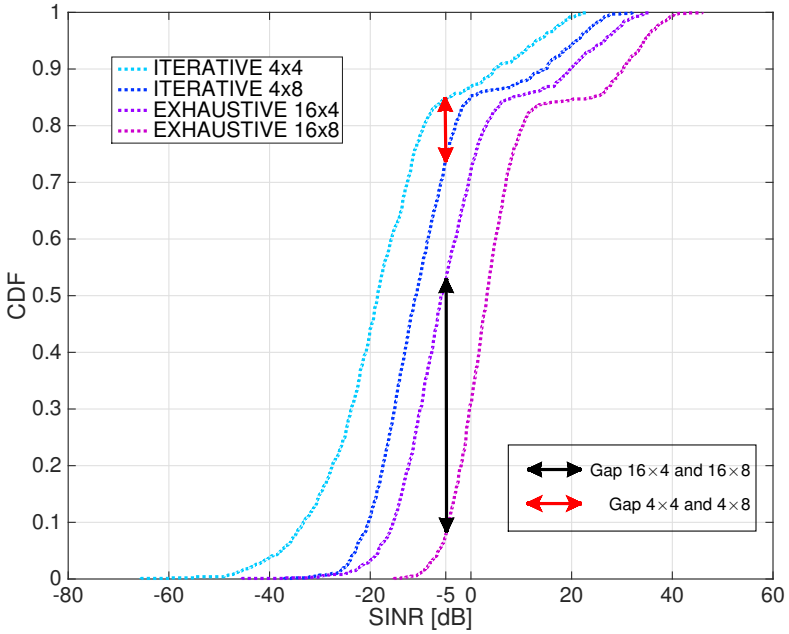

Fig. 6.2: Cumulative Distribution Function (CDF) of SINR for the 4 CS configurations. Distance $d = 120$ m. Insight when SINR $= -5$ dB.

exhaustive 16×4 and *exhaustive* 16×8. This depends on the intrinsic distribution of SINR, which follows the channel model described in [6] and varies according to the particular value of the BF gain.

6.2.3 Miss-detection probability

Figure 6.3 plots the miss-detection probability of both exhaustive and iterative CS techniques, when UE receives in either 4 or 8 directions, varying the distance between BS and user, from 0 to 200 meters. We want to highlight the goodness of each algorithm, in terms of detection probability, that is the probability that a UE within the cell is detected by the BS with SINR above threshold (set to -5 dB).

According to Figure 6.1, the lower the number of antennas at both UE and BS (scanning through fewer directions in reception or transmitting through wider beams), the lower the BF gain, the lower the SINR perceived by the UE and the higher the probability that this SINR is below the threshold τ. Despite their poor performance in terms of discovery time, exhaus-

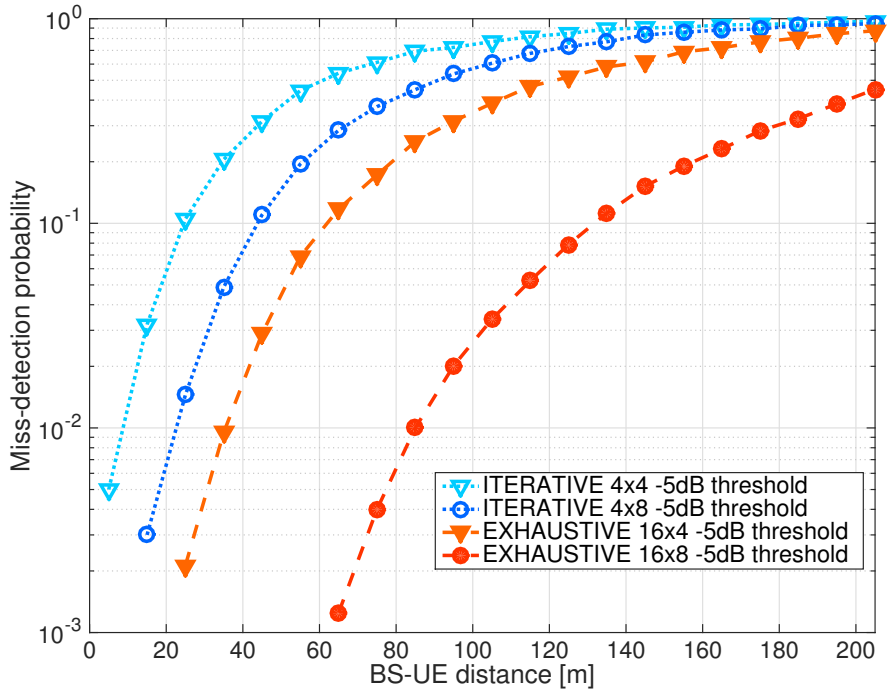

Fig. 6.3: P_{MD} for exhaustive and iterative techniques, when UE receives in either 4 or 8 directions, varying distance BS-UE. SINR threshold $\tau = -5$ dB.

tive algorithms directly scan in 16 narrow 22.5° sectors instead of 4 wide 90° ones and then outperform iterative techniques, from the miss-detection probability point of view. Therefore, there exist regions of the cell where a UE would be detected by the BS if exhaustive search is implemented, while it would not, if an iterative algorithm were used. Note that this happens even if a UE would be detected in the iterative second phase (when narrow beams are steered) but is outside the iterative first phase's range and thus cannot be found.

Again, the best performance is achieved implementing *exhaustive* 16×8 scheme, while *iterative* 4×4 scheme shows the maximum inefficiency.

In the range $0 \div 30$ meters, almost all algorithms present acceptable miss-detection probability values. At these distances, LoS condition is very likely met, pathloss is low and then P_{MD} is sufficiently small even when exploiting iterative searches. Therefore, when considering cells having very small radius, it may not be worthy to implement exhaustive procedures,

which are affected by high discovery delay, since iterative ones already present acceptable levels of detection[1].

Similarly, in the range $100 \div 200$ meters, almost all algorithms present unacceptable miss-detection probability values. In these regions, curves of Figure 6.3 have more or less the same behaviour and even overlap. This is due to the fact that, most of the times, UE would be in NLoS or even outage condition and the negative offset that takes care of these bad propagation characteristics can be more influential than the BF gain achieved by exhaustive techniques, which therefore also exhibit high values of P_{MD}. It is advisable to reduce the cell radius, in order to overcome the miss-detection phenomenon that UEs at cell edges would suffer.

In the range $30 \div 100$ meters, the possibility that a UE could be detected depends heavily on the implemented algorithm. A trade-off between discovery time and miss-detection probability can be useful to find the best CS technique.

We also notice that the *exhaustive* 16×8 curve is very detached from the *exhaustive* 16×4 one (and especially more detached than is the *iterative* 4×8 with respect to *iterative* 4×4). Let's consider, for example, a user at distance $d = 120$ m from its BS. According to considerations made for Figure 6.2, at -5 dB, a substantial difference in the gap between 16×4 and 16×8 and 4×4 and 4×8 is registered, due to the probability distribution of SINR, for different techniques.

Finally, in Figure 6.4, there are represented again the miss-detection probabilities of both exhaustive and iterative techniques, when receiving in 4 directions and varying, together with the distance from the BS, also the SINR thresholds.

As we expected, exhaustive technique outperforms iterative one. Anyway, when reducing the threshold from 0 to -5 to -10 dB, P_{MD} also decreases, since now a UE can be discovered also when it perceives a lower SINR value. Of course, there are needed optimal and more sophisticated reception techniques that can deal with more corrupted signals. It can be useful to analyse when it is really worthy to implement such enhancements.

[1] Consequently, at these distances, it may not be necessary to scan in 8 directions (increasing the BF gain at the expense of increasing the search time) since 4-directions reception can already guarantee good performance.

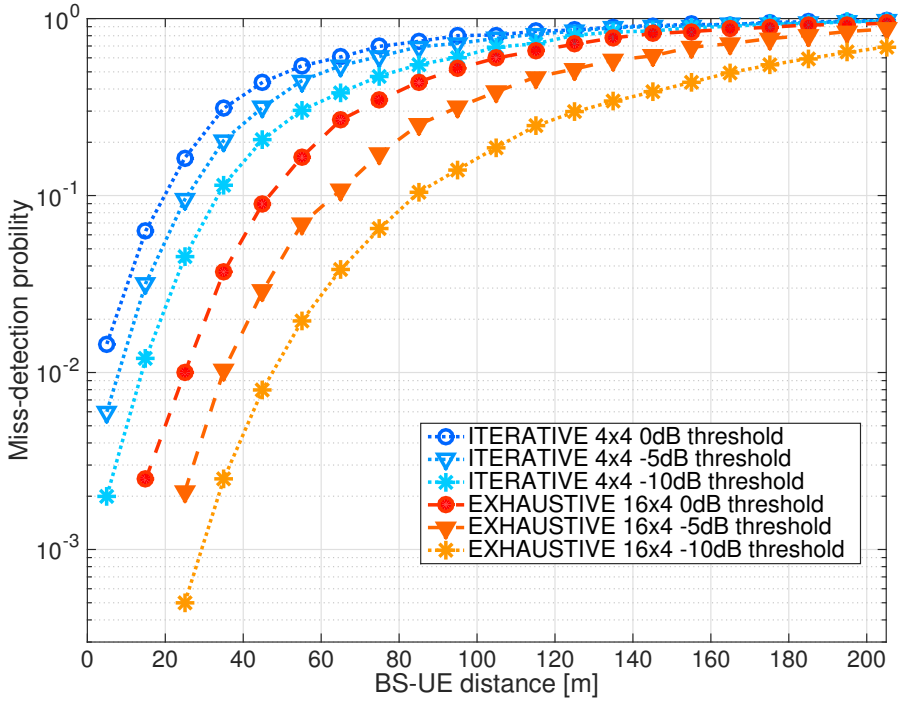

Fig. 6.4: P_{MD} for exhaustive and iterative techniques, when UE receives in 4 directions, varying distance BS-UE and SINR threshold.

Again, when the cell radius is very small, it is not worth reducing the threshold, since miss-detection is acceptable also when $\tau = 0$ dB. When the radius is very big (above 100 m), all procedures are almost equivalent and designing a more complex receiving scheme cannot recover P_{MD} to acceptable levels. Moreover, NLoS offset ($\simeq$ 20 dB) or outage offset ($\simeq$ 300 dB) are likely added at this range and completely overshadow the threshold reduction gain (around 5 or 10 dB), which is therefore ineffective and useless.

6.2.4 Miss-detection probability and CS slot duration

In this section, we study how the miss-detection probability varies, when changing the Cell-Search slot duration, whose default value is $T = 104\,\mu s$. The basic idea is that, if T is increased, the BS transmits its PSS for a longer time on the same sector and UEs belonging to that sector can perceive an increased received power. This results in increasing the SINR too and, con-

sequent, in reducing P_{MD}. The following equation,

$$SNR = \frac{E_b}{N_0} \tag{6.2}$$

identifies the energy per bit to noise power spectral density ratio; E_b is the signal energy associated with each user data bit while N_0 is the noise spectral density, and are both measured in Joule ($W \cdot s$). Equation (6.2) proves that the longer the transmission, the higher the SINR.

In this thesis, increasing the CS slot duration is simulated by lowering down the SINR threshold τ. In such a way, if the slot duration is doubled, the perceived SINR also doubles and this is equal to reduce τ by 3 dB. In fact, the power ratio corresponding to a 3 dB change in level is given by:

$$G = 10^{3/10} \simeq 1.99526 \approx 2 \tag{6.3}$$

We evaluate P_{MD} for three different UE's positions, varying T according to Table 6.3. $\tilde{T}$ refers to the *normalized CS slot duration*, thus $\tilde{T} = 1$ refers to the default duration ($T = 104\,\mu s$, with $\tau = -5$ dB), $\tilde{T} = 1/2$ means that duration is halved ($T = 52\,\mu s$), $\tilde{T} = 2$ reflects in doubling the slot length ($T = 208\,\mu s$), and so on.

Normalized slot duration $\tilde{T}$	**CS slot duration** T	**SINR Threshold** τ (dB)
$1/4$	$26\,\mu s$	1 dB
$1/2$	$52\,\mu s$	-2 dB
1	$104\,\mu s$	-5 dB
2	$208\,\mu s$	-8 dB
4	$416\,\mu s$	-11 dB

Table 6.3: Parameters for simulation of P_{MD} versus T. Grey row refers to default values.

Figure 6.5 plots the miss-detection probability, when UE is deployed at 30 meters from the BS, versus different values of the normalized CS slot duration $\tilde{T}$. We see that, when $\tilde{T}$ increases, P_{MD} inversely decreases since UEs can collect power for a longer time (E_b in (6.2) grows) and then perceive

higher SINR. The drawback is the higher discovery delay. As always, better performance is granted implementing exhaustive searches and receiving through more directions. We see also that curve for *exhaustive* 16×8 scheme is not within y-axis ranges since, at the current distance, P_{MD} is very small ($< 10^{-3}$) for all values of $\tilde{T}$.

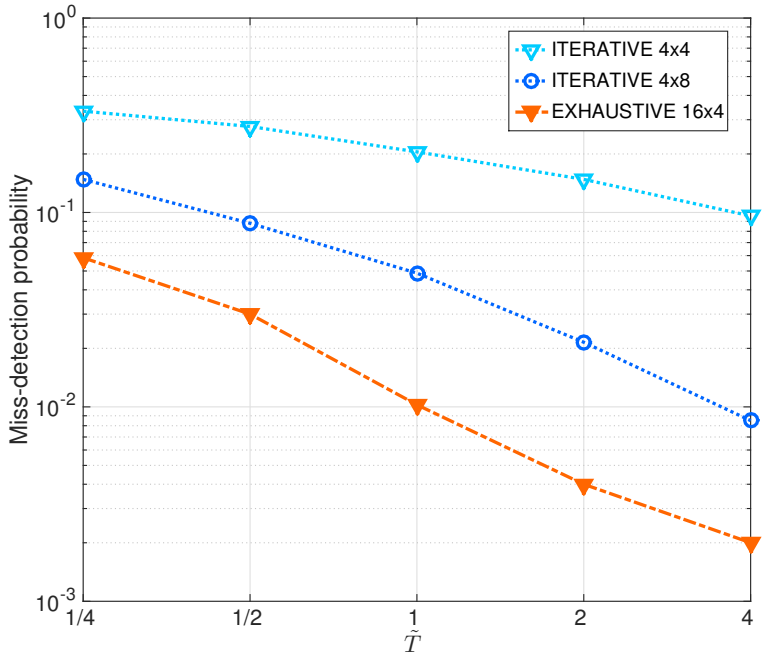

Fig. 6.5: P_{MD} for exhaustive and iterative techniques, versus normalized CS slot duration $\tilde{T}$. BS-UE distance $d = 30$ m.

Figure 6.6 reports the P_{MD}, when UE is deployed at 70 meters from the BS. Of course, miss-detection is higher since UE is further than the previous case, then it suffers from higher pathloss. This time, curves are closer to each other since enhancements due to increased slot period are balanced by worse mmW channel propagation characteristics. Again, it is remarkable the big gap between schemes 16×4 and 16×8, as already widely analysed before.

Finally, Figure 6.7 reports P_{MD} when UE is 140 m far form the BS. Here we note that, as already stated before, miss-detection probability does not show any relevant enhancement, when increasing $\tilde{T}$, and it stabilises to unacceptable levels. It does not worth increasing the discovery time and smaller cell radii must be considered, to improve edge users' performances. Again, only *exhaustive* 16×8 scheme presents a discrete behaviour.

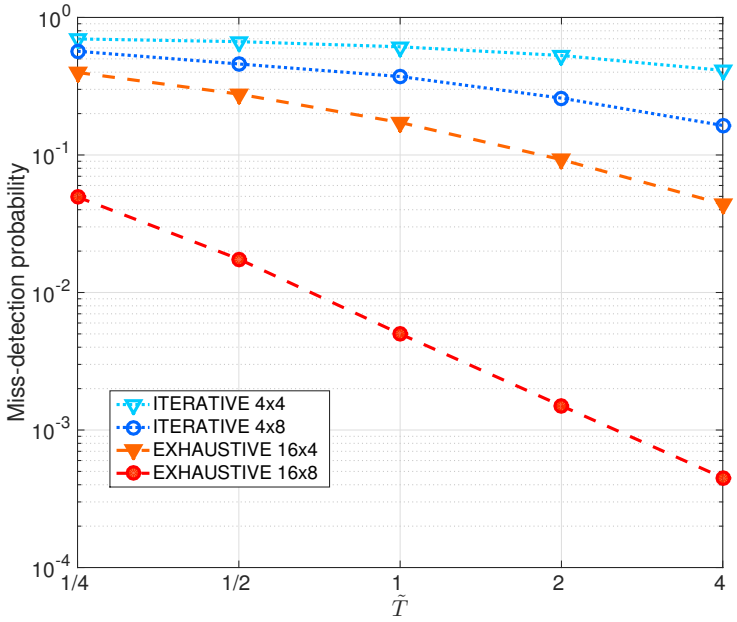

Fig. 6.6: P_{MD} for exhaustive and iterative techniques, versus normalized CS slot duration $\tilde{T}$. BS-UE distance $d = 70$ m.

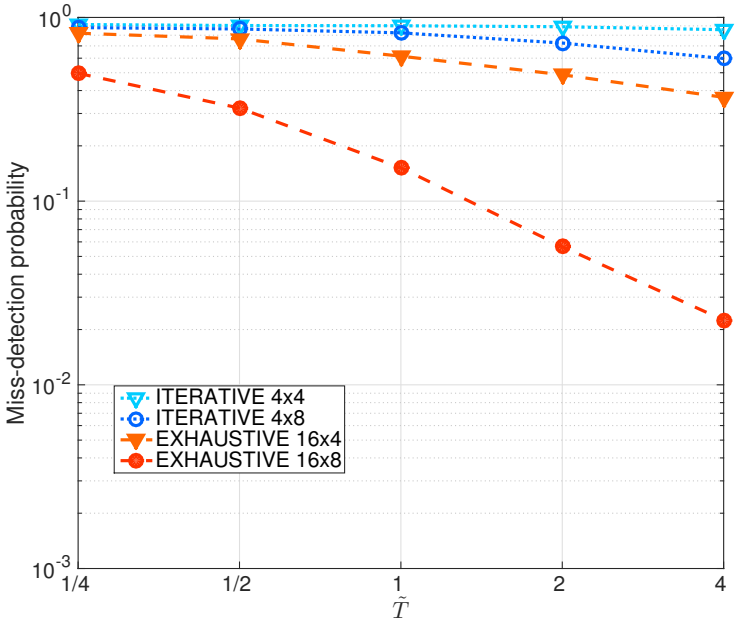

Fig. 6.7: P_{MD} for exhaustive and iterative techniques, versus normalized CS slot duration $\tilde{T}$. BS-UE distance $d = 140$ m.

Our goal is to find the best configuration to minimize the discovery time together with the miss-detection probability. We clearly see that these two aspects are irreconcilable since curves in the figures above do not have any minimum points. Therefore, a trade-off between CS slot duration and P_{MD} must be considered.

6.3 Comparisons and further analysis

In this section, we summarise pros and cons of each CS technique.

Iterative CS 4×4 Implementing this algorithm, it is not possible to perform AoA estimations, since receiving beams are not wider than transmitting ones, then UE will always communicate through 90° sectors, also after CS. Since the user cannot fully exploit its beamforming gain, throughput will be limited and data will be sent less efficiently. Moreover, very low BF gain leads to high P_{MD}: UEs at cell edges cannot be found, especially for relatively big cell radii. Despite these issues, UEs search is performed very quickly.

Iterative CS 4×8 Reception is performed through 8 narrow beams, then the UE's best transmit direction coincides with the best receiving one. In this way, after CS's second phase, a full antenna array can be exploited and throughput is maximised. This choice slows down the discovery, with respect to the 4×4 case, but higher BF gain reduces the miss-detection.

Exhaustive 16×4 Although reception is performed through 4 wide beams, AoA estimation algorithms can be used to compute the best 45° sector to reach the BS (since the receiving beam is wider than the transmitting one). This permits to achieve high throughput values, when communicating after CS, but it must be taken into account the computational complexity that AoA estimation requires. Cell-Search delay is considerable, but P_{MD} is sufficiently low, especially for small radius cells.

Exhaustive 16×8 This is the best possible solution to minimise the miss-detection probability and increase the discoverable area, since all 64 and 16 antenna elements of BS and UE, respectively, are used. Throughput is

of course maximised, after CS. The main drawback of this technique is the very high discovery delay: BS not only has to scan through 16 narrow directions, but also has to try many combinations to rendezvous with one of the 8 UE reception beams.

In Table 6.4, the trade-off among different CS procedures is reported.

Procedure	**Discovery time**	$P_{\mathbf{MD}}$	**Throughput after CS**
Iterative 4×4	Very low	Very high	Medium[(a)]
Iterative 4×8	Low	High	High
Exhaustive 16×4	High[(b)]	Low	High[(c)]
Exhaustive 16×8	Very high	Very low	High

(a) After CS, UE still transmits through 90° beams.
(b) But high computational complexity of AoA estimation.
(c) After AoA estimation.

Table 6.4: Trade-off table among different CS algorithms.

Among the described drawbacks, we highlight that the iterative technique is not recommended when dealing with very dense networks. When a UE is detected on a certain macro direction, after the first phase, this sector is consequently refined. If multiple users are found on *different* macro directions, it is necessary to refine all of them, one at a time. In this way, discovery can last more than in exhaustive techniques, and even with a worse miss-detection probability, due to low first phase BF gain. It is advisable to implement such an iterative procedure only when the users' arrival rate is low and when the probability that multiple UEs are under the coverage area of different macro sector is negligible.

Finally, we have seen that, when considering small cell radii (< 30 m), iterative procedures present sufficiently low values of P_{MD} and it is not

worth increasing the discovery time implementing exhaustive searches. Moreover, when dealing with very big cells (> 100 m), all techniques misbehave and again it's not convenient to increase the computational complexity with more expensive schemes, when they would show bad performances too.

Chapter 7

Conclusions and future works

In this thesis, we have studied and analysed possible implementations of Cell-Search techniques for upcoming 5G millimeter-wave cellular network.

After having outlined the main 5G requirements, key enabling technologies and limitations, we have reviewed the concept of Cell-Search and Initial-Access for current 4G-LTE systems, referring to the challenges the new 5G techniques will have to face.

We have also described the NS-3 framework, developed by the NYU research group, that we used to simulate our procedures, with particular reference to the physical layer. Then we have illustrated two particular CS techniques for future mmW networks, an exhaustive and an iterative procedure, analysing the modification we have made to the NS-3 modules, in order to simulate their performance.

Different NS-3 scenarios have been set, for comparing the CS algorithms performances under many metrics. A trade-off between discovery delay and miss-detection probability has been obtained.

Results show that iterative techniques are faster than exhaustive ones, since they do not need to scan the whole space, but they are limited to a specific 90° direction. Moreover, wide beams steered in the first phase reflects in lower BF gain and consequent higher miss-detection probability, with respect to exhaustive procedures, which in turn guarantee a wider discovery area. Among all the proposed solutions to reduce P_{MD}, at the expenses of increasing the discovery time, we can: (i) receive in 8 directions (instead of just 4), to increase the BF, (ii) increase the CS slot duration, (iii) similarly lower down the SINR threshold. Moreover, cell radius might be

reduced, so that users will perceive higher SINR values.

We can conclude that these two algorithms present opposite, but both fundamental, strengths that must be taken into account, depending on the network features, when researching on Cell-Search topic.

As part of our future work, we foresee to keep improving the NS-3 modules, as a joint effort with the NYU group we plan to work with. New and more sophisticated functionalities will be added to the framework, in order to simulate CS procedures in a more realistic way.

From a theoretical point of view, Cell-Search algorithms will be studied in detail and different implementation choices will be analysed. For example, in order to reconcile the low discovery time goal together with low miss-detection probability, digital beamforming can be realized, in order to steer multiple narrow beams simultaneously, at the expense of higher system complexity.

Moreover, CS procedures where HetNets are exploited deserve a deep investigation. Some works have already been published, like the ones in [50]. However, a lot of issues are still unsolved and research is just starting.

Furthermore, statistical analysis may be conducted, in order to simulate how users are distributed in the cell, what is their behaviour and arrival rate, to identify the best discovery procedure that fits the network requirement with the highest performance.

Many companies and research institutes are examining new possible standards for upcoming 5G networks, to overcome LTE limitations. Our future works are expected to pursue this action line.

Bibliography

[1] Cisco, "Cisco visual networking index: Global mobile data traffic forecast update, 2014–2019," Feb. 2015, White Paper. [Online]. Available at http://www.cisco.com/c/en/us/solutions/collateral/service-provider/visual-networking-index-vni/white_paper_c11-520862.pdf.

[2] Nokia, "Looking ahead to 5G," May 2014, White Paper. [Online]. Available at http://networks.nokia.com/file/28771/5g-white-paper.

[3] L. DMC R&D Center, Samsung Electronics Co., "5G vision," Feb. 2015, White Paper. [Online]. Available at http://www.samsung.com/global/business-images/insights/2015/Samsung-5G-Vision-0.pdf.

[4] F. Khan and Z. Pi, "mmWave mobile broadband (MMB): Unleashing the 3-300 GHz spectrum," in *Sarnoff Symposium, 2011 34th IEEE*, May 2011, pp. 1–6.

[5] S. Sesia, I. Toufik, and M. Baker, *LTE, The UMTS Long Term Evolution: From Theory to Practice*. Wiley Publishing, 2009.

[6] M. R. Akdeniz, Y. Liu, S. Sun, S. Rangan, T. S. Rappaport, and E. Erkip, "Millimeter wave channel modeling and cellular capacity evaluation," *CoRR*, vol. abs/1312.4921, 2013. [Online]. Available: http://arxiv.org/abs/1312.4921

[7] P. Kyösti, J. Meinilä, L. Hentilä, X. Zhao, T. Jämsä, C. Schneider, M. Narandzić, M. Milojević, A. Hong, J. Ylitalo, V.-M. Holappa, M. Alatossava, R. Bultitude, Y. de Jong, and T. Rautiainen,

"WINNER II Channel Models," Sep. 2007. [Online]. Available: http://www.ist-winner.org/deliverables.html

[8] G. Intellicence, "Understanding 5G: Perspectives on future technological advancements in mobile," Dec. 2014, White Paper. [Online]. Available at https://gsmaintelligence.com/research/?file=141208-5g.pdf&download.

[9] Huawei, "5G: A technology vision," Jan. 2014, White Paper. [Online]. Available at http://www.huawei.com/5gwhitepaper/.

[10] T. Rappaport, R. Heath, R. Daniels, and J. Murdock, *Millimeter Wave Wireless Communications*, ser. Communication engineering and emerging technologies. Prentice Hall, 2014. [Online]. Available: https://books.google.it/books?id=_Tt_BAAAQBAJ

[11] 5G-PPP, "5G vision," Feb. 2015, White Paper. [Online]. Available at https://5g-ppp.eu/wp-content/uploads/2015/02/5G-Vision-Brochure-v1.pdf.

[12] "NS-3 network simulator," [Online]. Available at http://www.nsnam.org.

[13] A. Damnjanovic, J. Montojo, Y. Wei, T. Ji, T. Luo, M. Vajapeyam, T. Yoo, O. Song, and D. Malladi, "A survey on 3GPP heterogeneous networks," *Wireless Communications, IEEE*, vol. 18, no. 3, pp. 10–21, June 2011.

[14] L. Wei, R. Hu, Y. Qian, and G. Wu, "Key elements to enable millimeter wave communications for 5G wireless systems," *Wireless Communications, IEEE*, vol. 21, no. 6, pp. 136–143, December 2014.

[15] E. Larsson, O. Edfors, F. Tufvesson, and T. Marzetta, "Massive MIMO for next generation wireless systems," *Communications Magazine, IEEE*, vol. 52, no. 2, pp. 186–195, February 2014.

[16] P. Banelli, S. Buzzi, G. Colavolpe, A. Modenini, F. Rusek, and A. Ugolini, "Modulation formats and waveforms for 5G networks: Who will be the heir of OFDM?: An overview of alternative modulation schemes for improved spectral efficiency," *Signal Processing Magazine, IEEE*, vol. 31, no. 6, pp. 80–93, Nov 2014.

[17] Y. Jarraya, T. Madi, and Debbabi, "A survey and a layered taxonomy of software-defined networking," *Communications Surveys Tutorials, IEEE*, vol. 16, no. 4, pp. 1955–1980, Fourthquarter 2014.

[18] H. Hawilo, A. Shami, M. Mirahmadi, and R. Asal, "NFV: state of the art, challenges, and implementation in next generation mobile networks," *Network, IEEE*, vol. 28, no. 6, pp. 18–26, Nov 2014.

[19] E. Hossain and M. Hasan, "5G cellular: key enabling technologies and research challenges," *Instrumentation Measurement Magazine, IEEE*, vol. 18, no. 3, pp. 11–21, June 2015.

[20] Z. Pi and F. Khan, "An introduction to millimeter-wave mobile broadband systems," *Communications Magazine, IEEE*, vol. 49, no. 6, pp. 101–107, June 2011.

[21] Mobile and wireless communications Enablers for the Twenty-twenty Information Society (METIS), "Intermediate description of the spectrum needs and usage principles," Aug 2013, document Number: ICT-317669-METIS/D5.1.

[22] S. Geng, J. Kivinen, X. Zhao, and P. Vainikainen, "Millimeter-wave propagation channel characterization for short-range wireless communications," *Vehicular Technology, IEEE Transactions on*, vol. 58, no. 1, pp. 3–13, Jan 2009.

[23] E. Dahlman, S. Parkvall, J. Skold, and P. Beming, *3G Evolution, Second Edition: HSPA and LTE for Mobile Broadband*, 2nd ed. Academic Press, 2008.

[24] Q. Li, H. Niu, G. Wu, and R. Hu, "Anchor-booster based heterogeneous networks with mmwave capable booster cells," in *Globecom Workshops (GC Wkshps), 2013 IEEE*, Dec 2013, pp. 93–98.

[25] H. Shokri-Ghadikolaei, C. Fischione, G. Fodor, P. Popovski, and M. Zorzi, "Millimeter wave cellular networks: A MAC layer perspective," *Communications, IEEE Transactions on*, 2015, 10.1109/TCOMM.2015.2456093.

[26] D. Liu, Y. Chen, K. K. Chai, and T. Zhang, "Joint uplink and downlink user association for energy-efficient hetnets using Nash bargaining

solution," in *Vehicular Technology Conference (VTC Spring), 2014 IEEE 79th*, May 2014, pp. 1–5.

[27] W.-C. Liao, M. Hong, and Z.-Q. Luo, "Max-min network flow and resource allocation for backhaul constrained heterogeneous wireless networks," in *Acoustics, Speech and Signal Processing (ICASSP), 2014 IEEE International Conference on*, May 2014, pp. 845–849.

[28] S. Sadr and R. S. Adve, "Handoff rate and coverage analysis in multi-tier heterogeneous networks," *CoRR*, vol. abs/1501.01668, 2015. [Online]. Available: http://arxiv.org/abs/1501.01668

[29] N. Baldo, M. Miozzo, M. Requena-Esteso, and J. Nin-Guerrero, "An open source product-oriented LTE network simulator based on ns-3," in *Proceedings of the 14th ACM International Conference on Modeling, Analysis and Simulation of Wireless and Mobile Systems*, ser. MSWiM '11. New York, NY, USA: ACM, 2011, pp. 293–298. [Online]. Available: http://doi.acm.org/10.1145/2068897.2068948

[30] "NYU wireless," available at http://nyuwireless.com.

[31] M. Mezzavilla, S. Dutta, M. Zhang, M. R. Akdeniz, and S. Rangan, "5G mmwave module for ns-3 network simulator," *CoRR*, vol. abs/1506.08801, 2015. [Online]. Available: http://arxiv.org/abs/1506.08801

[32] A. Ghosh, T. Thomas, M. Cudak, R. Ratasuk, P. Moorut, F. Vook, T. Rappaport, G. MacCartney, S. Sun, and S. Nie, "Millimeter-wave enhanced local area systems: A high-data-rate approach for future wireless networks," *Selected Areas in Communications, IEEE Journal on*, vol. 32, no. 6, pp. 1152–1163, June 2014.

[33] S. Dutta, M. Zhang, R. Ford, M. Mezzavilla, S. Rangan, and M. Zorzi, "Design and analysis of an ultra-low latency millimeter wave cellular MAC," To be submitted.

[34] T. Levanen, J. Pirskanen, and M. Valkama, "Dense small-cell networks: Rethinking the radio interface beyond LTE-advanced," in *5G for Ubiquitous Connectivity (5GU), 2014 1st International Conference on*, Nov 2014, pp. 163–169.

[35] M. Jankiraman, *Space-time Codes and MIMO Systems*, ser. Artech House universal personal communications series. Artech House, 2004. [Online]. Available: https://books.google.it/books?id=HU-T7y16AGEC

[36] S. Sun, T. Rappaport, R. Heath, A. Nix, and S. Rangan, "MIMO for millimeter-wave wireless communications: beamforming, spatial multiplexing, or both?" *Communications Magazine, IEEE*, vol. 52, no. 12, pp. 110–121, December 2014.

[37] A. Alkhateeb, O. El Ayach, G. Leus, and R. Heath, "Hybrid precoding for millimeter wave cellular systems with partial channel knowledge," in *Information Theory and Applications Workshop (ITA), 2013*, Feb 2013, pp. 1–5.

[38] C. N. Barati, S. A. Hosseini, S. Rangan, P. Liu, T. Korakis, and S. S. Panwar, "Directional cell search for millimeter wave cellular systems," *CoRR*, vol. abs/1404.5068, 2014. [Online]. Available: http://arxiv.org/abs/1404.5068

[39] C. Jeong, J. Park, and H. Yu, "Random access in millimeter-wave beamforming cellular networks: issues and approaches," *Communications Magazine, IEEE*, vol. 53, no. 1, pp. 180–185, January 2015.

[40] V. Desai, L. Krzymien, P. Sartori, W. Xiao, A. Soong, and A. Alkhateeb, "Initial beamforming for mmwave communications," in *Signals, Systems and Computers, 2014 48th Asilomar Conference on*, Nov 2014, pp. 1926–1930.

[41] Y. M. Tsang, A. S. Y. Poon, and S. Addepalli, "Coding the beams: Improving beamforming training in mmwave communication system," *CoRR*, vol. abs/1104.1007, 2011. [Online]. Available: http://arxiv.org/abs/1104.1007

[42] A. Capone, I. Filippini, and V. Sciancalepore, "Context-based cell search in millimeter wave 5G networks," *CoRR*, vol. abs/1501.02223, 2015. [Online]. Available: http://arxiv.org/abs/1501.02223

[43] K. Chandra, R. V. Prasad, I. G. Niemegeers, and A. R. Biswas, "Adaptive beamwidth selection for contention based access periods in millimeter wave WLANs," in *Consumer Communications and Networking Conference (CCNC), 2014 IEEE 11th*. IEEE, 2014, pp. 458–464.

[44] J. Singh and S. Ramakrishna, "On the feasibility of beamforming in millimeter wave communication systems with multiple antenna arrays," *CoRR*, vol. abs/1410.5509, 2014. [Online]. Available: http://arxiv.org/abs/1410.5509

[45] D. Ariananda and G. Leus, "Direction of arrival estimation of correlated signals using a dynamic linear array," in *Signals, Systems and Computers (ASILOMAR), 2012 Conference Record of the Forty Sixth Asilomar Conference on*, Nov 2012, pp. 2028–2035.

[46] Y. Tsang and A. Poon, "Successive aoa estimation: Revealing the second path for 60 GHz communication system," in *Communication, Control, and Computing (Allerton), 2011 49th Annual Allerton Conference on*, Sept 2011, pp. 508–515.

[47] P. A. Eliasi, S. Rangan, and T. S. Rappaport, "Low-rank spatial channel estimation for millimeter wave cellular systems," *CoRR*, vol. abs/1410.4831, 2014. [Online]. Available: http://arxiv.org/abs/1410.4831

[48] D. Lopez-Perez, I. Guvenc, G. de la Roche, M. Kountouris, T. Quek, and J. Zhang, "Enhanced intercell interference coordination challenges in heterogeneous networks," *Wireless Communications, IEEE*, vol. 18, no. 3, pp. 22–30, June 2011.

[49] S. A. Hosseini, C. N. Barati, M. Mezzavilla, P. Amir-Eliasi, S. Rangan, M. Zorzi, and S. S. Panwar, "Directional initial access for millimiter wave cellular systems."

[50] D. Liu, L. Wang, Y. Chen, M. Elkashlan, K. Wong, R. Schober, and L. Hanzo, "User association in 5G networks: A survey and an outlook," *CoRR*, vol. abs/1509.00338, 2015. [Online]. Available: http://arxiv.org/abs/1509.00338

Acknowledgements
Ringraziamenti

Per prima cosa, ci tengo a ringraziare i miei genitori, che da sempre mi sostengono con affetto e non mi fanno mai mancare nulla: dedico a loro questa tesi. Desidero ringraziare anche il mio relatore, Michele Zorzi, che mi sta dando la possibilità di interfacciarmi con un argomento affascinante come il 5G e che mi permette di essere fiero del lavoro fatto in questi anni di studio.

Grazie anche a tutte le persone che mi sono vicine e che continuano a supportami (e sopportarmi).

Grazie ai "più belli" Albe, Luci, Sere, Sophy, Gian, Matte, Eleonora, Ele, Gigi, Vero, Elisa, Pappa, Fra, Alberto, per i bellissimi momenti passati insieme e per farmi straviare, da anni, con la vostra simpatia e amicizia.

Grazie alla Ale, che dopo cinque anni di superiori ancora mi sta vicino come se non fosse passato neanche un giorno.

Grazie a Ire, sempre gentile e disponibile, come nessuno.

Grazie ai "compagni della Da" Bob, Giulia, Silvia, Chiara, Mary, Trinh, Meson, che sanno davvero cosa vuol dire fare quello che facciamo. Grazie a Bob che ha condiviso e condivide con me le fatiche di NS-3. Grazie a Bob e Giulia per i fantastici ricordi spagnoli.

Special thanks go also to Marco Mezzavilla, Menglei Zhang, Russell Ford, Dourjya Dutta and to the NYU research group, for their patience and assistance in helping me with the NS-3 framework: your support has been essential for my thesis, thanks for all your e-mails.

Grazie di cuore ad ognuno di voi.